Reviewed Preprint
v1 • September 29, 2025
Not revised

Reviewed Preprint
v2 • May 21, 2026
Revised by authors

Enterovirus D68 2A protease causes nuclear pore complex dysfunction and independently contributes to motor neuron toxicity

Katrina M Zinn[1,*], Mathew W McLaren[1,*], Michael T Imai[1], Malavika M Jayaram[1], Jeffrey D Rothstein[2], Matthew J Elrick[1,2]

[1]Hugo W. Moser Research Institute, Michael V. Johnston Center for Developmental Neuroscience, Kennedy Krieger Institute, Baltimore, United States • [2]Department of Neurology, Johns Hopkins School of Medicine, Baltimore, United States

For correspondence: elrick@kennedykrieger.org

[*] These authors contributed equally.

Competing interests: No competing interests declared

Funding: See page 24

Reviewing editor: John W Schoggins, The University of Texas Southwestern Medical Center, United States

eLife Assessment

This **valuable** study examines the cleavage of motor neuron nucleoporins by proteases of enterovirus D68, a pathogen associated with acute flaccid myelitis. The evidence supporting the effects of EV-D68 proteases on nuclear import and export is generally **solid**, as is the independent examination of EV-D68 protease on spinal cord neuron toxicity. The specific conclusions related to RNA export were considered overstated relative to the data presented.

https://doi.org/10.7554/eLife.108672.2.sa4

Abstract

The picornavirus Enterovirus D68 (EV-D68) is an important pathogen associated with acute flaccid myelitis (AFM). The pathogenesis of AFM involves infection of spinal motor neurons and motor neuron death, however the mechanisms linking EV-D68 infection to selective neurotoxicity are not well understood. Dysfunction of the nuclear pore complex (NPC) has been implicated in motor neuron injury in neurodegenerative diseases such as amyotrophic lateral sclerosis, and the NPC is also modified by picornavirus proteases during the course of infection. We therefore sought to determine the impact of EV-D68 proteases on NPC composition and function. We demonstrate widespread disruption of NPC composition by EV-D68 2A and 3C proteases via the direct cleavage of a relatively small number of nucleoporins, notably Nup98 and POM121 by $2A^{pro}$. Using reporter systems, we demonstrate that $2A^{pro}$ inhibits nuclear import and export of protein cargoes and also disrupts the permeability barrier of the NPC, while having no apparent effect on RNA export. Independently, we show that $2A^{pro}$ is toxic to induced pluripotent stem cell derived motor neurons by demonstrating a rescue of toxicity with $2A^{pro}$ inhibitor telaprevir at concentrations that are insufficient to inhibit viral replication. These findings expand our understanding of EV-D68 neuropathogenesis and provides a rationale for studying the NPC or $2A^{pro}$ as therapeutic targets in AFM.

Introduction

Enterovirus D68 (EV-D68) has caused multiple outbreaks of severe respiratory disease and the polio-like disorder acute flaccid myelitis (AFM) during the past decade. Though much work has been done to demonstrate the association between EV-D68 and AFM and to characterize the molecular evolution of EV-D68 leading to the increased virulence of contemporary strains, the mechanisms underlying its neuropathogenesis remain poorly understood (Elrick et al. 2021). EV-

D68 has been shown to infect spinal motor neurons in mouse models (Hixon et al. 2017) and human autopsy tissue (Vogt et al. 2022), and the dysfunction or death of motor neurons is thought to be the proximate cause of paralysis in AFM.

EV-D68 is a member of the family *Picornaviridae*, which have a non-enveloped icosahedral capsid and a single-stranded positive sense RNA genome (Oberste et al. 2004). Picornaviruses alter the composition and function of the nuclear pore complex (NPC) during the course of their life cycle (reviewed in Lizcano-Perret and Michiels 2021). The purpose for this is felt to be twofold. First, it allows for the redistribution of nuclear proteins such as Sam68 (McBride et al. 1996), polypyrimidine tract binding protein (Back et al. 2002), and the La protein (Meerovitch et al. 1993) to the cytoplasm, where they participate in the translation or replication of viral RNA. Second, it may disrupt nuclear translocation of transcription factors that mediate innate immunity, including interferon response factor 3 (Delhaye et al. 2004) and nuclear factor κB (Watters et al. 2017).

The NPC is a macromolecular structure greater than 100 MDa in size constructed in 8-fold symmetry from subunits known as nucleoporins (Nups). The NPC includes a symmetric core that is comprised of transmembrane Nups that anchor the NPC to the nuclear envelope, inner and outer rings, and a central channel. The central channel consists primarily of phenylalanine-glycine (FG) repeat domains contributed by multiple Nups that confer an intrinsically disordered structure. The central channel creates a permeability barrier against passive diffusion of macromolecules 40 kDa and larger. The central channel also permits active nucleocytoplasmic transport (NCT). NCT is mediated by transport adapters known as importins and exportins which interact with FG-repeats and require a Ran-GTP/Ran-GDP gradient across the nuclear envelope. On the nuclear face of the NPC resides the nuclear basket, which has roles in chromatin organization and RNA quality control, while the cytoplasmic face is adorned with cytoplasmic filaments that are important for transport receptor docking and remodeling of ribonucleoproteins during their export. (reviewed in Lin and Hoelz 2019)

Disruptions of nuclear import by picornaviruses were first reported in cells infected with poliovirus (PV) and coxsackievirus B3 (CV-B3) (Belov et al. 2000). These deficits were later correlated to cleavage of Nup153 and Nup62 during infection with PV (Gustin and Sarnow 2001) or human rhinovirus 14 (RV14) (Gustin and Sarnow 2002), implicating viral proteases in disruption of the NPC. PV 2A protease ($2A^{pro}$) was shown to disrupt the permeability barrier of the NPC, allowing passive diffusion across the nuclear lamina (Belov et al. 2004). RV 3C and 3CD proteases were found to impair nuclear import (Ghildyal et al. 2009). There have been conflicting reports as to whether or not PV $2A^{pro}$ activity also impairs RNA export (Park et al. 2008, Castello et al. 2009). The list of Nups targeted by enterovirus proteases was expanded to include Nup98 by PV $2A^{pro}$ (Park et al. 2008) and RanBP2, Nup214, and Nup153 by RV $3C^{pro}$ and $3CD^{pro}$ (Ghildyal et al. 2009). A further study in PV-infected cells demonstrated cleavage of Nup98, Nup153, TPR, Nup96, Nup58, Nup35, RanBP2, Nup214, and POM121, without attributing cleavage events to specific proteases (Krull et al. 2010). The cleavage of Nup62 (Park et al. 2010) and Nup98 (Park et al. 2015) by RV2 were found to selectively remove the FG-repeat domain, signifying a potential mechanism for the disruption of transport functions or of the NPC permeability barrier.

Interestingly, though all picornaviruses studied to date alter the NPC, the specific Nup targets and functional outcomes vary between strains. Amongst several RV strains, there were differential kinetics for the degradation of Nup98, Nup153, and Nup62 by $2A^{pro}$. Most strikingly, some strains showed little or no cleavage of Nup62 while it was efficiently degraded by others (Watters and Palmenberg 2011). Further, the consequences of Nup degradation vary amongst RV strains, showing differential effects on trafficking mediated by various transport receptors including importin-αβ, transportin 1, transportin 3, or Crm1/exportin 1 (Watters et al. 2017). This suggests that the impact of infection by specific picornavirus strains have unique effects on which cargoes are mislocalized, and on the relative balance of import vs export deficits. These differences may have implications for the efficiency of viral replication as well as the potential deleterious effects on host cells.

Few studies have attempted to comprehensively survey the impact of a picornavirus infection on the NPC. A proteomic analysis in cells overexpressing CVB3 $2A^{pro}$ identified several interacting partners of $2A^{pro}$ and showed that eukaryotic translation initiation factor 4G (eIF4G) and Nup98 were the most rapidly cleaved host proteins. This was associated with bidirectional deficits of nucleocytoplasmic transport and redistribution of nuclear mRNA into cytoplasmic stress granules (Serganov et al. 2022).

Disruption of the nuclear pore complex has been implicated in degenerative disorders of the motor neuron. In *C9orf72*-related amyotrophic lateral sclerosis (ALS), three independent screens identified deficits of nucleocytoplasmic transport contributing to neurodegeneration (Freibaum et al. 2015, Jovicic et al. 2015, Zhang et al. 2015). These results have since been extended to sporadic ALS (Coyne et al. 2021) and other neurodegenerative disorders including Huntington, Alzheimer, and Parkinson diseases (Grima et al. 2017, Eftekharzadeh et al. 2018, Shani et al. 2019). Furthermore, mutations in multiple Nup genes are sufficient to cause neurodegeneration, including several motor neuron diseases of childhood (Juhlen and Fahrenkrog 2018).

Given the well-established role of NPC dysfunction in both picornavirus infection and neurotoxicity, and the similarity of disrupted nucleocytoplasmic transport dysfunction in these settings, we wondered whether NPC dysfunction may be a mechanistic link between EV-D68 infection and neurotoxicity. As a first step in this line of inquiry, we sought to comprehensively characterize the impact of EV-D68 proteases on NPC composition and function, and to determine the contribution of EV-D68 proteases to motor neuron toxicity in models of AFM. Here, we show that $2A^{pro}$ is primarily responsible for wide-ranging deficits of nucleocytoplasmic transport of protein cargoes via cleavage of a small number of Nups, and is neurotoxic in induced pluripotent stem cell (iPSC)-derived human spinal motor neurons.

Results

Enterovirus D68 proteases disrupt nuclear pore complex composition

We screened for disruption of the nuclear pore complex by expressing in HEK293T cells the $2A^{pro}$ and $3C^{pro}$ proteases from US/MO/2014-18947, a well-characterized neuropathogenic strain of EV-D68 that has been studied in animal and cell culture models of AFM (Liu et al. 2015, Brown et al. 2018, Hixon et al. 2019). We measured the levels of 30 nucleoporins in whole cell lysates by Western blot. As positive controls, we used the homologous proteases from poliovirus 1 Mahoney strain. To confirm protease activity, we also measured the levels of EIF4G (Ventoso et al. 1998) and CREB (Yalamanchili et al. 1997), well-established non-Nup substrates of $2A^{pro}$ and $3C^{pro}$, respectively. After correction for multiple comparisons, we identified 14 Nups whose levels were decreased after expression of EV-D68 $2A^{pro}$ and four Nups whose levels were decreased after expression of $3C^{pro}$, revealing a widespread disruption of NPC composition following EV-D68 protease expression. In addition, Western blots showed putative cleavage products of three Nups for each protease that were detectable only in the presence of protease (Figure 1A-B). Including these proteins, our total list of candidate Nup substrates of EV-D68 proteases numbered 15 for $2A^{pro}$ (RanBP2, Nup214, Nup88, Aladin, Gle1, Nup43, Nup96, Nup188, Nup35, POM121, Nup62, Nup54, Nup98, TPR, Nup153) and 6 for $3C^{pro}$ (RanBP2, Nup214, Nup188, Nup35, NDC1, Nup50).

We considered that alterations in the level of each Nup may be either a direct result of proteolytic cleavage, or a secondary effect such as loss of a binding partner in the complex. We therefore sought to determine which of the candidate Nups are substrates of their respective EV-D68 protease. We performed *in vitro* assays of proteolytic cleavage for each Nup of interest by incubating HEK293T cell nuclear-fractionated lysates with recombinant $2A^{pro}$ or $3C^{pro}$ and quantifying Nup levels over time by Western blot. All candidate Nups were detectable by this method with the exception of Nup43, which was excluded from further analysis. Surprisingly, of the 14 remaining candidate substrates of $2A^{pro}$, only Nup98 and POM121 were significantly

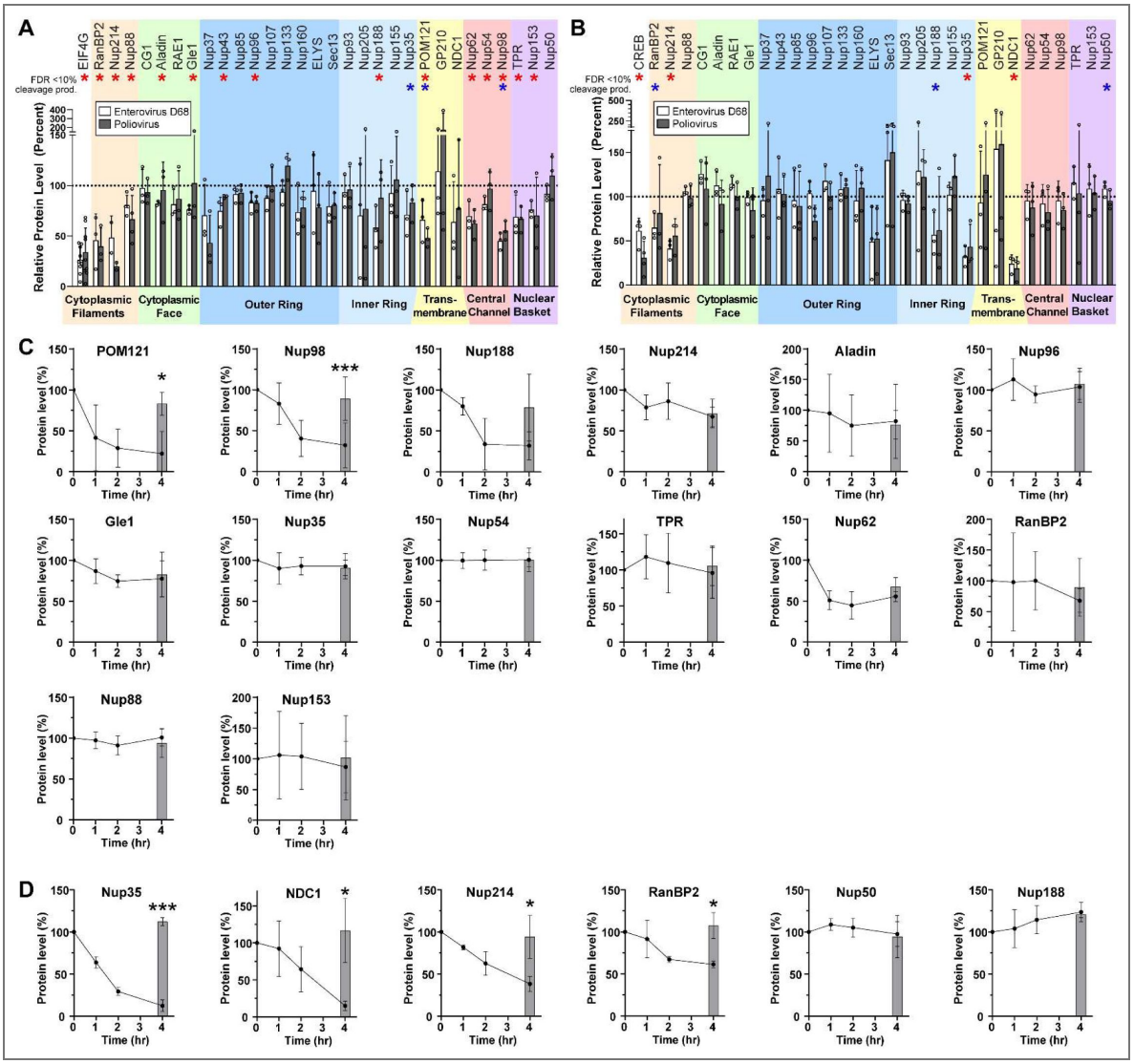

Figure 1. Enterovirus D68 proteases cleave several nucleoporins.

(A) HEK cells were transfected with Enterovirus D68 2A^{pro}, Poliovirus 1 2A^{pro}, or empty vector control, and the indicated nucleoporins were quantified by western blot, normalized to control=100%. EIF4G was included as a non-nucleoporin positive control. Mean ± S.D. of 3 independent replicates. Statistical comparison was by multiple t-tests of the EV-D68 2Apro vs control, with multiple comparisons correction by the false discovery rate method. Red asterisks represent significance with FDR<10%, blue asterisks represent samples for which a cleavage product was visible on the Western blot irrespective of significance. (B) As in A, except transfecting with 3C^{pro}. The positive control was CREB. (C) Nuclear lysates from HEK cells were incubated at 37°C with recombinant EV-D68 2A^{pro} at a ratio of 1:50 (protease:lysate by mass) for the indicated time. Grey bars represent lysate incubated for 4 hours at 37°C in the absence of protease as a negative control. Mean ± S.D. of 3 independent replicates. Statistical comparison was by t-test between the with- and without-protease samples at 4 hours. (D) As in C, except with EV-D68 3C^{pro} at a ratio of 1:200. *p<0.05, **p<0.01, ***p<0.001.

proteolyzed in these nuclear preparations (Figure 1C). For $3C^{pro}$, four out of six candidates demonstrated significant evidence of proteolysis, including Nup35, NDC1, Nup214, and RanBP2 (Figure 1D).

2A protease alters nucleocytoplasmic trafficking of protein substrates

We next sought to understand the functional impacts of Nup cleavage and altered NPC composition on nucleocytoplasmic transport. We began by screening for steady state alterations of nucleocytoplasmic localization using a reporter system based on the previously reported Shuttle-tdTomato (Zhang et al. 2015). We expressed NLS-tdTomato, tdTomato-NES, or Shuttle-tdTomato (which we will refer to henceforth as NLS-tdTomato-NES) in HeLa cells, followed by GFP-labeled versions of each of the EV-D68 proteases or an empty vector GFP control. NLS-tdTomato is typically localized to the nucleus and tdTomato-NES to the cytoplasm, serving as readouts of nuclear import and export, respectively. NLS-tdTomato-NES is transported bidirectionally with an approximately uniform nucleocytoplasmic distribution at steady state. Its localization is expected to change during altered nucleocytoplasmic transport only when there are unequal effects on nuclear import vs export. GFP-$2A^{pro}$-expressing cells demonstrated significant alterations, wherein the NLS-tdTomato and tdTomato-NES reporters were significantly less partitioned into the nucleus or cytoplasm (Figure 2A-C; Supplementary Figure 2).

The above findings have two potential explanations which are not mutually exclusive: (1) $2A^{pro}$ impairs receptor-mediated nuclear import and export, or (2) $2A^{pro}$ disrupts the permeability barrier of the NPC, allowing for passive diffusion of macromolecules across the nuclear envelope. To test the first of these possibilities, we utilized a photoinducible reporter system to measure the kinetics of nucleocytoplasmic transport. We used pDB22 (mCherry-LINus) for nuclear import (Niopek et al. 2014) and pDN122 (NLS-mCherry-LEXY) for nuclear export (Niopek et al. 2016). Both mCherry-LINus and NLS-mCherry-LEXY failed to translocate in HeLa cells following expression of $2A^{pro}$, but not $3C^{pro}$ (Figure 2D-E; Supplementary Figure 3). These findings demonstrate deficits in both nuclear import and nuclear export of protein cargoes induced by $2A^{pro}$.

2A protease disrupts the permeability barrier of the nuclear pore complex

To assess the integrity of the nuclear permeability barrier we measured the exclusion of a high molecular weight fluorescently labeled dextran from the nucleus (Lenart and Ellenberg 2006) following selective permeabilization of the plasma membrane with digitonin (Adam et al. 1990). As expected, in digitonin-permeabilized HeLa cells expressing an empty vector control or $3C^{pro}$, FITC-dextran diffused rapidly into the cytoplasm but was excluded from the nucleus. By contrast, in $2A^{pro}$-expressing cells FITC-dextran accumulated in the nucleus, indicating a disruption of the permeability barrier against diffusion of macromolecules (Figure 2F-G).

In sum, the above data indicate that disruption of the nuclear pore complex specifically by $2A^{pro}$ leads to deficits in bidirectional nucleocytoplasmic transport of protein cargoes as well as disruption of the NPC permeability barrier against passive diffusion. To exclude the possibility that these phenomena are simply non-specific sequelae of cell death, we measured the uptake of propidium iodide in GFP+ HeLa cells transfected with IRES-GFP, IRES-GFP-$2A^{pro}$, or IRES-GFP-$3C^{pro}$, imaged and analyzed identically to those in the tdTomato and LINus/LEXY reporter assays, and found no significant increase in nuclear propidium iodide uptake between control and protease-expressing cells (Figure 2H).

Enterovirus D68 proteases do not disrupt RNA export

Given the substantial disruption of nucleocytoplasmic transport of protein cargoes by $2A^{pro}$, we next asked whether RNA export from the nucleus is similarly altered. We used two complementary measurements of RNA transport in HEK293T cells transfected with EV-D68

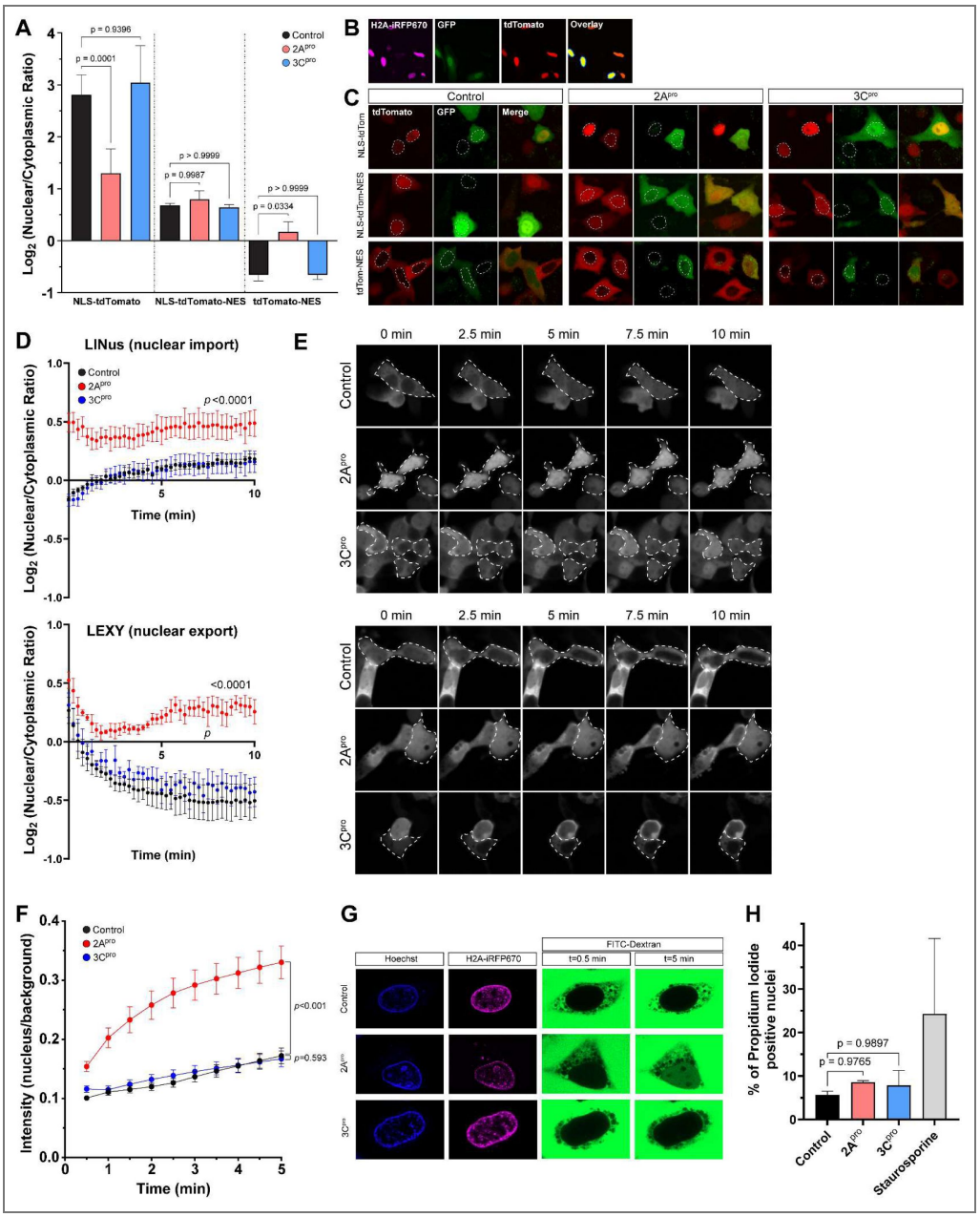

Figure 2. Enterovirus D68 2A protease impairs nucleocytoplasmic transport of protein cargoes and disrupts the nuclear pore complex permeability barrier.

(A) tdTomato reporter assay showing nuclear-cytoplasmic ratios at steady state 20 hours after transfection of IRES-GFP, IRES-GFP-2A^{pro}, or IRES-GFP-3C^{pro}. Mean values of three independent replicates *n*=29,404 GFP+ cells in total, error bars are S.D. Statistical comparison was by two-way ANOVA with Šídák's multiple comparisons test. (B) Example output of image analysis protocol. In the overlay image, yellow represents the nuclei of transfected cells, defined by the area of expression of H2A-iRFP670 in GFP+ cells only. The surrounding dark blue ring is the perinuclear cytoplasm. The intensity of reporter construct was measured in the red channel and reported as a ratio of nuclear to perinuclear cytoplasmic signal. (C) Example images from A. Dotted outlines mark the nuclei. (D) Kinetics of nuclear import (left) and export (right) measured by photoinducible LINus and LEXY reporter assays, respectively, in HeLa cells 20 hours after transfection with IRES-GFP, IRES-GFP-2A^{pro}, or IRES-GFP-3C^{pro}. Mean values of 3 biologically independent replicates, *n*=999 GFP+ cells for LINus and 1059 for LEXY in total. Error bars are S.E.M. Statistical comparison was by two-way ANOVA. (E) Example images from D. Dotted outlines mark GFP+ cells. (F) Dextran exclusion assay was performed in HeLa cells 15 hours after transfection with IRES-iRFP670-H2A, IRES-iRFP670-H2A-(2A)-2A^{pro}, or IRES- iRFP670-H2A-(2A)-3C^{pro}. *n*=45-46 cells per group pooled from 3 biologically independent replicates. Statistical comparison was by two-way ANOVA. (H) Propidium iodide viability assay. Mean values of 3 independent replicates, *n*=8042 cells in total. Error bars are S.D. Statistical comparison was by one-way ANOVA with Tukey's multiple comparison test.

proteases: Poly-A RNA-FISH to label the steady-state distribution of native mRNA, and 5-ethinyl uridine (EU) pulse chase labeling of nascent RNAs to measure the kinetics of RNA export. In the case of the latter experiment, we also used combinations of RNA polymerase inhibitors actinomycin D, α-amanitin, and CAS 577784-91-9 to selectively label the products of RNA polymerase I, II, or III. In all cases, there was no significant alteration of nuclear-cytoplasmic localization of RNA (Figure 3A-C; Supplementary Figure 4). We also performed the EU pulse-chase assay in RD cells infected with EV-D68. To control for potential strain-specific effects, we used EV-D68 strains from two different subclades and outbreak years, US/MO/2014-18947 (clade B1, year 2014) and US/MD/2018-23209 (clade B3, year 2018) (Figure 3D-E).

Enterovirus D68 infection recapitulates the effect of 2A protease on nucleocytoplasmic transport

We next sought to determine whether key deficits seen during transfection of recombinant proteases were also present during live virus infection. We also focused most of these experiments on a disease-relevant cell type, human iPSC-derived spinal motor neurons (diMNs), using multiple independent iPSC lines to control for the potential variability of these cells. We found that Nup98 and POM121 levels were decreased by EV-D68 infection in a similar manner as $2A^{pro}$-transfected cell lines, and this was at least partially reversed by the $2A^{pro}$ inhibitor telaprevir in a dose-dependent manner (Figure 4A). We also evaluated whether nucleocytoplasmic transport disruption occurs during live virus infection by performing the NLS-tdTomato and tdTomato-NES reporter assays in RD cells infected with EV-D68. These cells demonstrated disrupted localization of both markers, and the deficits were rescued in a concentration-dependent fashion by telaprevir. (Figure 4B-C) In diMNs, there was a strong disruption NLS-tdTomato localization in response infection but little if any alteration of tdTomato-NES localization in diMNs. The mislocalization of NLS-tdTomato was partially rescued by 3μM telaprevir. (Figure 4D-E)

Inhibition of 2A protease rescues the toxicity of Enterovirus D68 to spinal motor neurons out of proportion to its potential antiviral effect

In the above experiments, we demonstrated that EV-D68 $2A^{pro}$ disrupts the composition of the nuclear pore complex and has deleterious consequences on the maintenance of the NPC permeability barrier and nuclear transport of protein cargoes in cell lines and human spinal motor neurons. We next sought to determine the extent to which $2A^{pro}$ activity independently contributes to motor neuron injury during EV-D68 infection. GFP-labeled diMNs were infected with EV-D68 and imaged daily by high content imaging with automated cell counting. These diMNs demonstrated gradual yet robust cell death in culture. The EV-D68 $2A^{pro}$ inhibitor telaprevir led to a dose-dependent reduction in cell death, with statistically significant neuroprotection occurring at concentrations of 0.3μM and above (Figure 4F-G). We considered the possibility that the rescue of nucleocytoplasmic transport deficits and motor neuron toxicity may simply be due to an antiviral effect of telaprevir. However, the growth curve of EV-D68 in diMNs showed modest inhibition by telaprevir that achieved statistical significance in only one of two strains at a concentration of 10μM, and in neither strain at lower concentrations (Figure 4H). We therefore infer that telaprevir protects motor neurons from EV-D68-induced cell death primarily because it inhibits the effects of $2A^{pro}$ activity on host targets.

Discussion

Here we have presented a detailed evaluation of the effects of EV-D68 proteases on the composition and function of the NPC. Our findings on Nup cleavage are compatible with previous findings in other picornaviruses, and extend the literature by presenting one of the most comprehensive evaluations of Nups to date. Interestingly, we found widespread disruption of the NPC by EV-D68 proteases. The levels of up to 16 Nups were decreased by one or both proteases. By contrast, only 6 Nups were found to be direct proteolytic substrates of $2A^{pro}$ or $3C^{pro}$. This finding

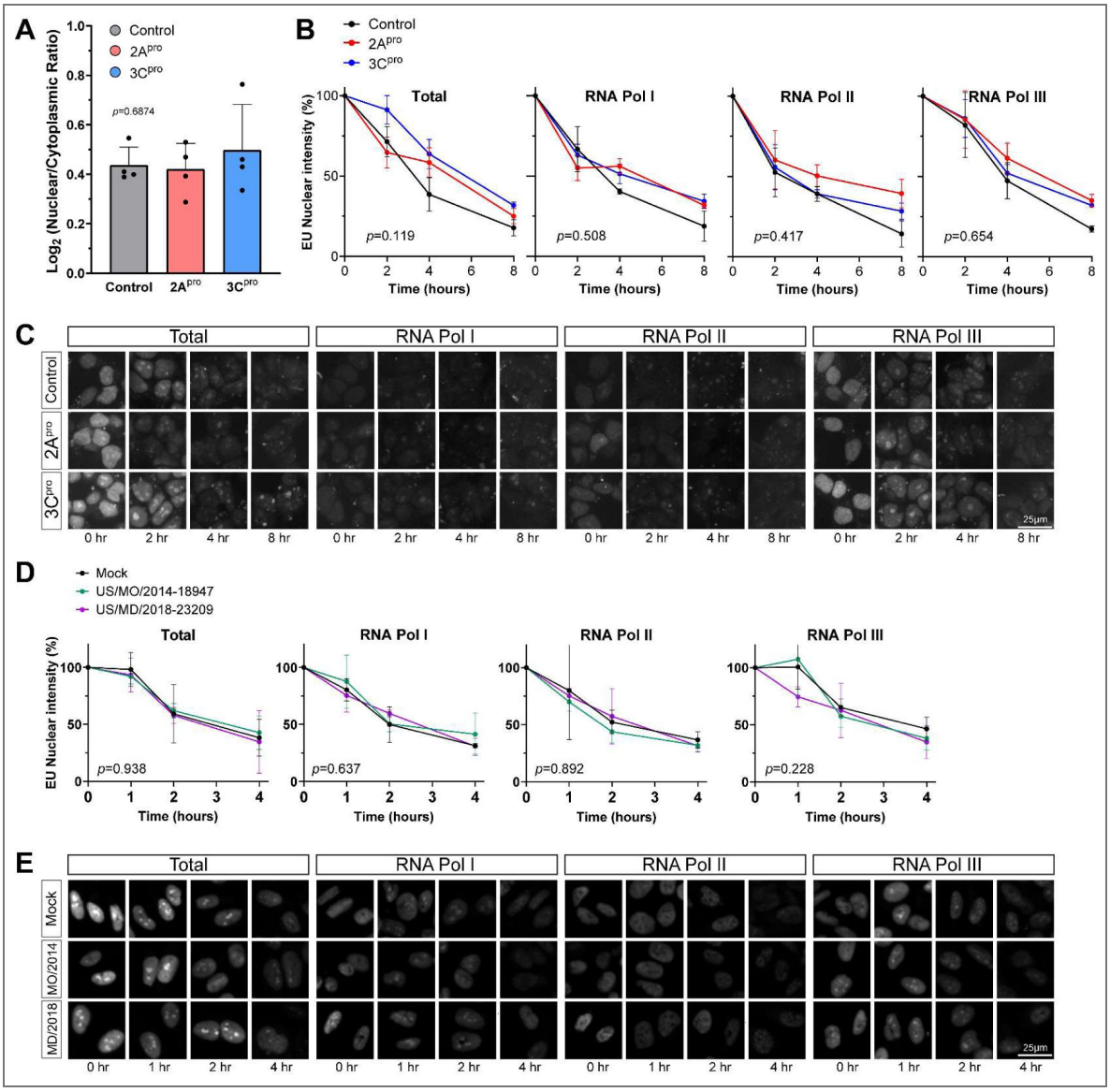

Figure 3. Enterovirus D68 proteases do not significantly alter RNA export.

(A) Steady state mRNA levels were measured by Poly-A FISH in HeLa cells 20 hours after transfection with IRES-GFP, IRES-GFP-2A^{pro}, or IRES-GFP-3C^{pro}. Data represent the mean ± S.D. of four independent replicates, *n*=55,177 GFP+ cells in total. Statistical comparison was by one-way ANOVA with Šídák's multiple comparisons test. (B) Nuclear export of EU-labeled RNAs in HEK cells by 1hr pulse followed by 0-8hr chase. EU labeling began 20hr after transfection with IRES-GFP, IRES-GFP-2A^{pro}, or IRES-GFP-3C^{pro}. Pulse labeling of total RNA or primarily the products of the listed RNA polymerases was performed in the presence of pairs of combinations of actinomycin D, α-amanitin, and CAS 577784-91-9 as described in Materials and Methods. Data represent the mean ± S.E.M. of three independent replicates. *n*=253,015 GFP+ cells analyzed in total. Statistical comparison was by two-way ANOVA. (C) Representative images from the experiment described in B. (D) Nuclear export of EU-labeled RNAs in RD cells by 1hr pulse followed by 0-4hr chase. EU labeling began 24 hours after infections with EV-D68 strains at MOI 5 or mock infection as indicated. Data represent the mean ± S.E.M. of three independent replicates. *n*=125,401 cells analyzed in total. Statistical comparison was by two-way ANOVA. (E) Representative images from the experiment described in D.

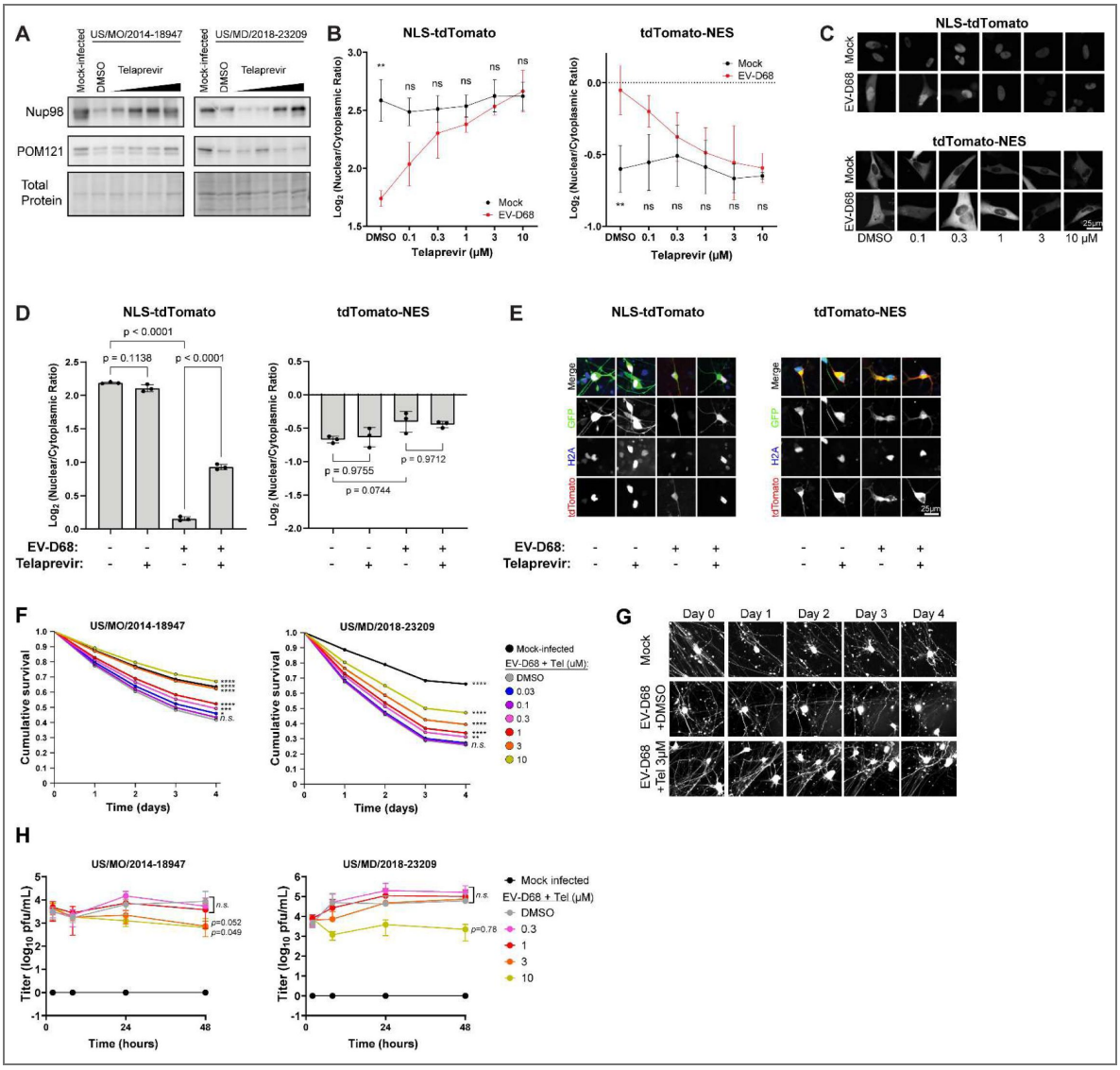

Figure 4. Effects of 2A protease during Enterovirus D68 infection on NPC function and motor neuron toxicity.

(A) Western blots of diMN lysates collected 24 hours after infection with the indicated strains of EV-D68 at MOI 5 followed by treatment with telaprevir at 0.3, 1, 3, and 10 μM. Total protein loading control was Biorad stainfree imaging. One representative example out of three biologically independent replicates. (B) tdTomato reporter assays in RD cells showing nuclear-cytoplasmic ratios 24 hours after mock infection or infection with EV-D68 US/MO/2014-18947. Telaprevir was added following infection at the indicated concentrations. Data are mean of three independent replicates, *n*=11,847 cells in total for NLS-tdTomato and *n*=8941 for tdTomato-NES. (C) Representative images of tdTomato signal from B. (D) tdTomato reporter assays in diMN showing nuclear-cytoplasmic ratios 24 hours after mock infection or infection with EV-D68 US/MO/2014-18947, treated with DMSO or 3μM telaprevir. Means of three replicates from independent iPSC lines. *n*=3388 cells in total for NLS-tdTomato and. *n*=3371 for tdTomato-NES. (E) Representative images from panel D. (F) Survival of diMNs following infection with EV-D68 at MOI 5 with the indicated EV-D68 strains in the presence of varying concentrations of telaprevir or DMSO control. diMNs were generated from four independent iPSC lines. *n*=8512 and 7046 cells counted for US/MO/2014-18947 and US/MD/2018-23209 respectively. Statistical comparisons were by Cox proportional hazard regression. (G) Representative images of diMNs from the experiment presented in panel F. Note fragmentation of neurites and loss of cell body shape signifying cell death following EV-D68 infection, and relative preservation following treatment with 3μM telaprevir. (H) Growth curve of EV-D68 in the presence of varying concentrations of telaprevir or DMSO control. Infections were performed with the indicated strains at MOI 0.5, using diMNs generated from four independent iPSC lines for each virus. Error bars are SEM. Statistical comparisons were by two-way ANOVA with Dunnet's multiple comparisons test between DMSO and telaprevir-treated groups. **p*<0.05, ***p*<0.01, ****p*<0.001, *****p*<0.0001.

suggests that the remaining Nup alterations may be a secondary effect. For example, some of the altered Nups may be anchored to the NPC by other Nups which are themselves targets for proteolysis.

Our study also provides a mechanistic explanation for disrupted localization of nucleocytoplasmic cargoes. By using several complementary reporter systems to detect abnormalities of nucleocytoplasmic transport dynamically and at steady state we showed that the deficits are multifactorial, resulting from both disruption of the NPC's permeability barrier against passive diffusion of macromolecules and from loss of receptor-mediated nuclear import and export.

It is striking that functional deficits in the NPC were entirely attributable to $2A^{pro}$, even though we only observed two definitive substrates of $2A^{pro}$: Nup98 and POM121. Nup98 has been well-studied as a target of picornavirus 2A proteases, though studies have drawn differing conclusions regarding the extent and nature of the impact of Nup98 cleavage on NPC function (Park et al. 2008, Castello et al. 2009, Serganov et al. 2022). The finding that $2A^{pro}$ also cleaves POM121 is especially interesting because of its role in motor neuron degeneration in ALS. POM121 appears to function as a "keystone" for the NPC. In models of ALS, removal of POM121 from the NPC is sufficient to cause loss of multiple Nups including Nup98, Nup107, Nup50, TPR, Nup133, GP210, and NDC1 (Coyne et al. 2020), a list that overlaps with what we observed following $2A^{pro}$ expression. In these ALS models, overexpression of POM121 is sufficient to reverse NPC deficits, and the mechanism of POM121 removal appears to be inappropriate activation of the ESCRT III pathway (Coyne et al. 2021, Coyne and Rothstein 2021, Baskerville et al. 2024). In the context of EV-D68 infection, it remains to be determined whether Nup98 or POM121 is the primary driver of NPC pathology, if the mechanism of POM121 loss involves the ESCRT pathway or is only due to its cleavage by $2A^{pro}$, and whether deficits of NPC function can be reversed via repair of Nups or prevention of their cleavage. These questions will be a focus of future studies.

We have also demonstrated that $2A^{pro}$ activity contributes to nucleocytoplasmic transport dysfunction and separately to cell death in motor neurons infected with EV-D68. Our approach was motivated by the fact that similar NPC deficits have been shown to be toxic in neurodegenerative disorders of the motor neuron. We therefore hypothesize that the $2A^{pro}$-dependent toxicity that we witnessed in diMNs is at least partially due to these deficits of NPC function. Concordant with our observation of $2A^{pro}$-dependent toxicity, a recent study demonstrated amelioration of the AFM phenotype in EV-D68-infected mice treated with telaprevir. The protection of spinal motor neurons in these mice occurred despite minimal effects on viral replication in the spinal cord, providing further support for a model in which telaprevir's mechanism of action is primarily neuroprotective rather than antiviral (Frost et al. 2023). A significant limitation of our study, however, is that we cannot exclude potentially toxic effects of $2A^{pro}$ on aspects of host neuronal biology aside from the NPC. For example, $2A^{pro}$ impairs 5'-cap-dependent RNA translation via eIF4G cleavage (Ventoso et al. 1998) and inhibits stress granule formation (Visser et al. 2019) which could also contribute to toxicity in EV-D68-infected neurons. Further work will be required to disentangle the relative contributions of these pathways to motor neuron injury.

Conclusion

We have built upon prior observations in several picornaviruses to show that EV-D68 proteases cause broad disruption of the composition and function of the nuclear pore complex, and that these phenomena are attributable to the cleavage of a relatively small number of Nups by $2A^{pro}$. Further, $2A^{pro}$ contributes to motor neuron death in a model of EV-D68 infection. These findings motivate future work to evaluate the NPC or $2A^{pro}$ as potential therapeutic targets to treat or prevent paralysis in AFM.

Materials and methods

Key Reagents

Primary Antibodies		
Antibody	**Manufacturer**	**Cat. No.**
2Apro	Biomatik	Custom produced rabbit polyclonal antibody against recombinant $2A^{pro}$ from US/MO/2014-18947
Aladin	Bethyl Laboratories	A304-514A
CG1 (NUPL2; Nup42)	Thermo	PA5-88035
CREB	Cell Signaling	9197
ELYS	Bethyl Laboratories	A300-166A
GAPDH	Abcam	ab8245
GFP	Takara Bio	632375
Gle1	Novus	NBP2-47449
GP210	Bethyl Laboratories	A301-795A
mAb414	Abcam	Ab24609
NDC1 (TMEM48)	Novus Biologicals	NBP1-91603
Nucleolin	Cell Signaling	14574S
Nup107	Thermo Fisher-Scientific	19217-1-AP
Nup133	Santa Cruz	sc-376699
Nup153	Abcam	Ab24700
Nup155	Abcam	ab199528
Nup160	Bethyl Laboratories	A301-790A
Nup188	Bethyl Laboratories	A302-323A-T
Nup205	Abcam	ab157090
Nup214	Abcam	ab70497
Nup35 (Nup53)	Proteintech	19819-1-AP
Nup37	Thermo Fisher-Scientific	PA5-66007
Nup43	Abcam	ab69447
Nup50	Santa Cruz	sc-398993
Nup54	Sigma Aldrich	HPA035929
Nup62	Millipore	MABE1043
Nup85	Proteintech	19370-1-AP
Nup88	Santa Cruz	sc-365868
Nup93	Santa Cruz	sc-374399
Nup96	Bethyl	A301-785A
Nup98	Abcam	ab50610
Nup98	Santa Cruz	sc-101546
POM121	GeneTex	GTX102128
RAE1	Santa Cruz	sc-393252
RanBP2	Santa Cruz	sc74518
RanBP2	Santa Cruz	sc74518
Sec13	Proteintech	15397-1-AP
SNAP29	Abcam	ab181151
TPR	Bethyl Laboratories	A300-828A
VP1	GeneTex	GTX132313
Secondary Antibodies		
Goat Anti-Mouse IgG H&L HRP	Abcam	ab205719
Goat Anti-Rabbit IgG H&L HRP	Abcam	ab205718
Goat Anti-Rat IgG H&L HRP	Abcam	ab205720
Goat anti-Mouse IgG (H+L) Highly Cross-Adsorbed Secondary Antibody, Alexa Fluor 488	Thermo Fisher	A32723

Plasmids Previously reported elsewhere	
Name	**Source**
pmTurquoise-H2A	Addgene 36207 (Goedhart et al. 2012)
FU-MAP2-Gateway	Addgene 43915 (Addis et al. 2011)
eBFP2-N1	Addgene 54595 (Michael Davidson)
pDB22 (mCherry-LINus)	Addgene 61342 (Niopek et al. 2014)
pDN122 (NLS-mCherry-LEXY)	Addgene 72655 (Niopek et al. 2016)
pLenti-DsRed-IRES-GFP	Addgene 92194 (Rousseaux et al. 2016)

hMAP2-pGreenZero	System Biosciences SR10047PA-1
Shuttle-tdTomato	(Zhang et al. 2015)
peSUMOstar	LifeSensors, Inc

Plasmids produced for this work

Name	Components	PCR Primers	Assembly Method
CMV-(EV-D68)2Apro	Backbone: NheI/AgeI digest of eBFP2-N1		In-Fusion Snap Assembly
	Insert: Synthetic DNA 1		
CMV-(EV-D68)3Cpro	Backbone: NheI/AgeI digest of eBFP2-N1		In-Fusion Snap Assembly
	Insert: Synthetic DNA 7		
CMV-(PV1)2Apro	Backbone: NheI/AgeI digest of eBFP2-N1		In-Fusion Snap Assembly
	Insert: Synthetic DNA 2		
CMV-(PV1)3Cpro	Backbone: NheI/AgeI digest of eBFP2-N1		In-Fusion Snap Assembly
	Insert: Synthetic DNA 8		
pLenti-IRES-GFP	AfeI/BamHI digest of pLenti-DsRed-IRES-GFP to linearize and remove DsRed		In-Fusion Snap Assembly
	PCR amplification of the above product	MJE_69, MJE_71	
	Recircularization via In-Fusion Snap Assembly		
pLenti-IRES-GFP-2Apro	Backbone: BsrGI digest of pLenti-IRES-GFP		In-Fusion Snap Assembly
	Insert: Synthetic DNA 11		
pLenti-IRES-GFP-3Cpro	Backbone: BsrGI digest of pLenti-IRES-GFP		In-Fusion Snap Assembly
	Insert: Synthetic DNA 12		
pLenti-IRES-H2A-iRFP	Backbone: BsrGI digest of pLenti-IRES-GFP to linearize, followed by PCR	MTI_1, MTI_7	In-Fusion Snap Assembly
	Insert: PCR amplificaion of H2A-iRFP from MAP2-H2A-iRFP670 with addition of P2A site	MTI_5, MTI_13	
pLenti-IRES-H2A-iRFP(P2A)2Apro	Backbone: BsrGI digest of pLenti-IRES-GFP-2A to linearize, followed by PCR	MTI_2, MTI_8	In-Fusion Snap Assembly
	Insert: PCR amplificaion of H2A-iRFP from MAP2-H2A-iRFP670 with addition of P2A site	MTI_5, MTI_13	
pLenti-IRES-H2A-iRFP(P2A)3Cpro	Backbone: BsrGI digest of pLenti-IRES-GFP-3C to linearize, followed by PCR	MTI_12, MTI_9	In-Fusion Snap Assembly
	Insert: PCR amplificaion of H2A-iRFP from MAP2-H2A-iRFP670 with addition of P2A site	MTI_5, MTI_13	
NLS-tdTomato	XhoI digest of Shuttle-tdTomato		In-Fusion Snap Assembly
	PCR amplificaton, followed by recircularization	MJE_10, MJE_11	
tdTomato-NES	MluI digest of Shuttle-tdTomato		In-Fusion Snap Assembly
	PCR amplificaton, followed by recircularization	MJE_8, MJE_53	
MAP2-pmTurqoise-H2A	Backbone: NdeI digest of pmTurquoise-H2A to linearize, followed by PCR amplification	KEB_1, KEB_2	In-Fusion Snap Assembly
	Insert: PCR amplification of FU-MAP2-Gateway	KEB_3, KEB_4	
MAP2-H2A-iRFP670	Backbone: AgeI/NotI digest of MAP2-pmTurqoise-H2A		T4 ligase
	Insert: Synthetic DNA 22, digested with AgeI/NotI		
peSUMOstar-2A^{pro}	Backbone: BsaI digest of peSUMOSTAR		In-Fusion Snap Assembly
	Insert: Synthetic DNA 23		

Primers

Name	Sequence
KEB_1	CGGAACTCCATATATGGGCTATGAACTAAT
KEB_2	GGTTTAGTGAACCGTCAGATCCGCA
KEB_3	ATATATGGAGTTCCGCAGCTGGCCTTTTTGGTTCTCAT
KEB_4	GGTTTAGTGAACCGTTCGGTTAGAGACAAGCTGAAGAATCTACCG

MJE_10	CTCGAGCAGAAACTCATCTCAGAAGAGGATC
MJE_11	TGAGTTTCTGCTCGAGCTGTAGCTTGTACAGCTCGTCCATGC
MJE_53	CATGCCCCCGCCTCCCATGGTGGCACGCGTCG
MJE_69	CACCGGCGGCCTAGCCGCCCCTCTC
MJE_70	CACCGGCGGCCTAGCAACCATGG
MJE_8	GGAGGCGGGGGCATGGTGAG
MTI_1	GAGAACCCTGGACCTTCTAGATAACTGATCCTCTCCC
MTI_12	GAGAACCCTGGACCTGGTCCAGGCTTCGGAGGAGTTTTTG
MTI_13	AGGTCCAGGGTTCTCCTCCACGTCGCCAGCCTGCTTCAGCAGGCTGAAGTTAGTAGCGCGTTGGTGGTGGG
MTI_2	GAGAACCCTGGACCTGGTCCAGGCTTCGG
MTI_5	AATATGGCCACAACCATGTCGGGACGTGGC
MTI_7	GAGAACCCTGGACCTGGACCAGG
MTI_8	GAGAACCCTGGACCTGGACCAGGGTTCG
MTI_9	GAGAACCCTGGACCTGGACCAGGGTTCGATT

Synthetic DNA	
Name	**Sequence**
1	GTCAGATCCGCTAGCGCCACCATGGGTCCAGGCTTCGGAGGAGTTTTTGTAGGGTCTTTTAAAATAATCAACTATCA CTTGGCCACTACAGAAGAGAGACAGTCAGCTATCTATGTGGATTGGCAATCAGACGTCTTGGTTACCCCCATTGCTG CTCATGGAAGGCACCAAATAGCAAGATGCAAGTGCAACACAGGGGTTTACTATTGTAGGCACAAAAACAGAAGTTAC CCGATTTGCTTTGAAGGCCCAGGGATTCAATGGATTGAACAAAATGAATATTACCCAGCAAGGTACCAGACCAATGT ACTTTTGGCAGTTGGTCCTGCGGAAGCAGGAGATTGCGGTGGTTTACTAGTTTGTCCACATGGGGTAATCGGTCTT CTTACAGCAGGAGGGGGTGGAATTGTAGCTTTCACTGATATCAGGAATTTGCTATGGTTAGATACTGATGCTATGGAA CAATGGGATCCACCGGTCG
2	GTCAGATCCGCTAGCGCCACCATGGGATTCGGACACCAAAACAAAGCGGTGTACACTGCAGGTTACAAAATTTGCA ACTACCACTTGGCCACTCAGGATGATTTGCAAAACGCAGTGAACGTCATGTGGAGTAGAGACCTCTTAGTCACAGA ATCAAGAGCCCAGGGCACCGATTCAATCGCAAGGTGCAATTGCAACGCAGGGGTGTACTACTGCGAGTCTAGAAG GAAATACTACCCAGTATCCTTCGTTGGCCCAACGTTCCAGTACATGGAGGCTAATAACTATTACCCAGCTAGGTACCA GTCCCATATGCTCATTGGCCATGGATTCGCATCTCCAGGGGATTGTGGTGGCATACTCAGATGTCACCACGGGGTG ATAGGGATCATTACTGCTGGTGGCGAAGGGTTGGTTGCATTTTCAGACATTAGAGACTTGTATGCCTACGAAGAAGA AGCCATGGAACAATGGGATCCACCGGTCG
7	GTCAGATCCGCTAGCGCCACCATGGGACCAGGGTTCGATTTTGCACAAGCCATAATGAAGAAAAATACCGTCATTG CAAGGACTGAAAAGGGTGAGTTCACCATGCTGGGTGTATATGATAGGGTAGCGGTCATCCCCACACACGCATCTGT TGGAGAAACCATTTACATTAATGATGTAGAGACTAAAGTTTTAGATGCGTGTGCACTTAGAGACTTGACTGATACAAA CTTAGAGATAACCATAGTCAAATTAGACCGTAATCAAAAATTTAGAGATATCAGACATTTTCTGCCCAGATATGAGGAT GATTACAATGACGCTGTGCTTAGCGTACATACATCAAAATTCCCAAATATGTATATCCCAGTTGGACAAGTCACCAATT ATGGCTTCTTGAACCTAGGTGGTACACCGACGCACCGCATTTTAATGTATAACTTCCCAACAAGAGCTGGCCAGTGT GGTGGTGTGGTGACAACTACAGGTAAGGTGATAGGAATACATGTAGGTGGAAATGGAGCTCAAGGATTTGCAGCAA TGCTACTACACTCTTACTTTTCCGATACACAAGGTGAGATAGTTAGTAGTGAAAAGAGTGGGGTGTGCATTAACGCA CCGGCAAAGACTAAACTCCAACCTAGTGTTTTCCATCAAGTTTTTTAATGGGATCCACCGGTCG
8	GTCAGATCCGCTAGCGCCACCATGGGACCAGGGTTCGATTACGCAGTGGCTATGGCTAAAAGAAACATTGTTACAG CAACTACTAGCAAGGGAGAGTTCACTATGTTAGGAGTCCACGACAACGTGGCTATTTTACCAACCCACGCTTCACCT GGTGAAAGCATTGTGATCGATGGCAAAGAAGTGGAGATCTTGGATGCCAAAGCGCTCGAAGATCAAGCAGGAACC AATCTTGAAATCACTATAATCACTCTAAAGAGAAATGAAAAGTTCAGAGACATTAGACCACATATACCTACTCAAATCA CTGAGACAAATGATGGAGTCTTGATCGTGAACACTAGCAAGTACCCCAATATGTATGTTCCTGTCGGTGCTGTGACT GAACAGGGATATCTAAATCTCGGTGGGCGCCAAACTGCTCGTACTCTAATGTACAACTTTCCAACCAGAGCAGGACA GTGTGGTGGAGTCATCACATGTACTGGGAAAGTCATCGGGATGCATGTTGGTGGGAACGGTTCACACGGGTTTGC AGCGGCCCTGAAGCGATCATACTTCACTCAGAGTCAATAATGGGATCCACCGGTCG
11	ATGGACGAGCTGTACAAGTCCGGACTCAGATCTCGAGCTCAAGCTTCGAATTCTGCAGTCGACGGTACCGCGGGC CCGGGTCCAGGCTTCGGAGGAGTTTTTGTAGGGTCTTTTAAAATAATCAACTATCACTTGGCCACTACAGAAGAGAG ACAGTCAGCTATCTATGTGGATTGGCAATCAGACGTCTTGGTTACCCCCATTGCTGCTCATGGAAGGCACCAAATAG CAAGATGCAAGTGCAACACAGGGGTTTACTATTGTAGGCACAAAAACAGAAGTTACCCGATTTGCTTTGAAGGCCCA GGGATTCAATGGATTGAACAAAATGAATATTACCCAGCAAGGTACCAGACCAATGTACTTTTGGCAGTTGGTCCTGC GGAAGCAGGAGATTGCGGTGGTTTACTAGTTTGTCCACATGGGGTAATCGGTCTTCTTACAGCAGGAGGGGGTGG AATTGTAGCTTTCACTGATATCAGGAATTTGCTATGGTTAGATACTGATGCTATGGAACAATAAGTACAAGTAATCTAG

12	ATGGACGAGCTGTACAAGTCCGGACTCAGATCTCGAGCTCAAGCTTCGAATTCTGCAGTCGACGGTACCGCGGGC CCGGGACCAGGGTTCGATTTTGCACAAGCCATAATGAAGAAAAATACCGTCATTGCAAGGACTGAAAAGGGTGAGT TCACCATGCTGGGTGTATATGATAGGGTAGCGGTCATCCCCACACACGCATCTGTTGGAGAAACCATTTACATTAATG ATGTAGAGACTAAAGTTTTAGATGCGTGTGCACTTAGAGACTTGACTGATACAAACTTAGAGATAACCATAGTCAAATT AGACCGTAATCAAAAATTTAGAGATATCAGACATTTTCTGCCCAGATATGAGGATGATTACAATGACGCTGTGCTTAG CGTACATACATCAAAATTCCCAAATATGTATATCCCAGTTGGACAAGTCACCAATTATGGCTTCTTGAACCTAGGTGGT ACACCGACGCACCGCATTTTAATGTATAACTTCCCAACAAGAGCTGGCCAGTGTGGTGGTGTGGTGACAACTACAG GTAAGGTGATAGGAATACATGTAGGTGGAAATGGAGCTCAAGGATTTGCAGCAATGCTACTACACTCTTACTTTTCCG ATACACAATAAGTACAAGTAATCTAG
22	ATGGCGCGTAAGGTCGATCTCACCTCCTGCGATCGCGAGCCGATCCACATCCCCGGCAGCATTCAGCCGTGCGGC TGCCTGCTAGCCTGCGACGCGCAGGCGGTGCGGATCACGCGCATTACGGAAAATGCCGGCGCGTTCTTTGGACG CGAAACTCCGCGGGTCGGTGAGCTACTCGCCGATTACTTCGGCGAGACCGAAGCCCATGCGCTGCGCAACGCAC TGGCGCAGTCCTCCGATCCAAAGCGACCGGCGCTGATCTTCGGTTGGCGCGACGGCCTGACCGGCCGCACCTTC GACATCTCACTGCATCGCCATGACGGTACATCGATCATCGAGTTCGAGCCTGCGGCGGCCGAACAGGCCGACAAT CCGCTGCGGCTGACGCGGCAGATCATCGCGCGCACCAAAGAACTGAAGTCGCTCGAAGAGATGGCCGCACGGGT GCCGCGCTATCTGCAGGCGATGCTCGGCTATCACCGCGTGATGTTGTACCGCTTCGCGGACGACGGCTCCGGGAT GGTGATCGGCGAGGCGAAGCGCAGCGACCTCGAGAGCTTTCTCGGTCAGCACTTTCCGGCGTCGCTGGTCCCGC AGCAGGCGCGGCTACTGTACTTGAAGAACGCGATCCGCGTGGTCTCGGATTCGCGCGGCATCAGCAGCCGGATC GTGCCCGAGCACGACGCCTCCGGCGCCGCGCTCGATCTGTCGTTCGCGCACCTGCGCAGCATCTCGCCCTGCCA TCTCGAATTTCTGCGGAACATGGGCGTCAGCGCCTCGATGTCGCTGTCGATCATCATTGACGGCACGCTATGGGGA TTGATCATCTGTCATCATTACGAGCCGCGTGCCGTGCCGATGGCGCAGCGCGTCGCGGCCGAAATGTTCGCCGAC TTCTTATCGCTGCACTTCACCGCCGCCCACCACCAACGCTAA
23	GAACAGATTGGAGGTGGTCCTGGTTTTGGTGGCGTCTTTGTGGGTTCTTTCAAAATAATTAACTACCACCTGGCGAC GACAGAGGAACGCCAATCAGCGATTTATGTTGACTGGCAAAGCGATGTCTTGGTTACCCCGATTGCAGCACACGGA CGTCACCAAATTGCCCGGTGTAAATGCAATACGGGAGTATATTATTGTAGACATAAGAACCGTAGTTACCCCATTTGTT TTGAAGGACCAGGCATCCAATGGATCGAGCAGAACGAGTACTACCCAGCCAGATACCAAACGAACGTACTGCTGGC GGTGGGTCCTGCGGAAGCTGGCGATTGTGGGGGCTTGTTGGTGTGTCCGCACGGCGTAATTGGATTACTGACTGC CGGGGGTGGTGGTATCGTGGCGTTTACTGATATTCGCAATCTTCTGTGGTTAGATACTGATGCCATGGAACAAtgatga CTAGAGGATCCGAAT

Cell culture media and solutions	
Complete Media (CM)	Dulbecco's modified Eagle Medium (Thermo Fisher 11995073) 10% fetal bovine serum (Thermo Fisher 16140071) 1% penicillin/streptomycin (Thermo Fisher 15140122) 2mM L-glutamine (Thermo Fisher 25030081) 1mM Sodium Pyruvate (Millipore Sigma S8636)
Infection Media (IM)	Dulbecco's modified Eagle Medium (Thermo Fisher 11995073) 2.5% fetal bovine serum (Thermo Fisher 16140071) 1% penicillin/streptomycin (Thermo Fisher 15140122) 2mM L-glutamine (Thermo Fisher 25030081) 1mM Sodium Pyruvate (Millipore Sigma S8636)
Stage 1 diMN Media (S1)	50% Iscove's Modified Dulbesso's Medium (IMDM) (Thermo Fisher 12440053) 50% Ham's F12 nutrient mix (Thermo Fisher 11765062) 1X Non-essential amino acids (Thermo Fisher 11140050) 1X Penicillin-Streptomycin (Thermo Fisher 15140122) 1X B27 Supplement (Thermo Fisher 17504044) 1X N2 Supplement (Thermo Fisher 17502048) 0.2μM LDN-193189 (Stemgent 04-0074) 10μM SB431542 (STEMCELL Technologies 72234) 3 μM CHIR99021 (Millipore Sigma SML1046)
Stage 2 diMN Media (S2)	50% IMDM (Thermo Fisher 12440053) 50% Ham's F12 nutrient mix (Thermo Fisher 11765062) 1X Non-essential amino acids (Thermo Fisher 11140050) 1X Penicillin-Streptomycin (Thermo Fisher 15140122) 1X B27 Supplement (Thermo Fisher 17504044) 1X N2 Supplement (Thermo Fisher 17502048) 0.2μM LDN-193189 (Stemgent 04-0074) 10μM SB431542 (STEMCELL Technologies 72234) 3 μM CHIR99021 (Millipore Sigma SML1046) 0.1μM All-trans retinoic acid (Millipore Sigma R2625) 1μM SAG (Cayman Chemicals 11914)
Stage 3 diMN Media (S3)	50% IMDM (Thermo Fisher 12440053) 50% Ham's F12 nutrient mix (Thermo Fisher 11765062) 1X Non-essential amino acids (Thermo Fisher 11140050) 1X Penicillin-Streptomycin (Thermo Fisher 15140122) 1X B27 Supplement (Thermo Fisher 17504044) 1X N2 Supplement (Thermo Fisher 17502048)
	0.1μM Compound E (Millpore Sigma 565790) 2.5μM DAPT (Millipore Sigma D5942) 0.1μM db-cAMP (Millipore Sigma 28745) 0.5μM All-trans retinoic acid (Millipore Sigma R2625) 1μM SAG (Cayman Chemicals 11914) 200ng/mL Ascorbic acid (Millipore Sigma A4544) 10ng/mL Brain-derived neurotrophic factor (PeproTech 450-02) 10ng/mL Glial cell-derived neurotrophic factor (PeproTech 450-10)
PBS+	Phosphate buffered saline (Gibco10010023) 100 g/L $MgCl_2$ (Sigma) 100 g/L $CaCl_2$ (Sigma)

Plasmid Construction

Plasmids were constructed from the components listed in the Key Reagents table using In-Fusion Snap Assembly (Takara Bio) or T4 DNA Ligase (New England Biolabs) following the manufacturers' protocol. The products of restriction digests and PCR reactions were purified using 1% agarose gel electrophoresis. The band of interest was visualized using SYBR Safe dye (Thermo Fisher) under blue light to avoid UV exposure, cut out of the gel, and recovered using the GeneJet Gel Extraction Kit (Thermo Fisher). Transfections of non-neuronal cell lines were performed using FuGene HD per the manufacturer's protocol (Promega). Transfection of motor neurons was by Lonza Nucleofection as described below. Of note, expression of EV-D68 proteases using a CMV promoter and a Kozak sequence as the ribosome binding site, while sufficient to introduce measurable protease activity (Figure S1), did not allow a sufficiently bright signal for imaging assays using fluorescently tagged proteases. This is a commonly encountered problem, owing to the inhibition of transcription and 5'-cap-dependent translation by enterovirus proteases, which we resolved by incorporating an internal ribosome entry site (IRES) in front of the fusion protein (Castello et al. 2006).

Viruses and titering

Viral strains were US/MO/2014-18947 (BEI Resources, NR-49129) and US/MD/2018-23209 (gift of Dr. Andrew Pekosz, Johns Hopkins Bloomberg School of Public Health). Viral stocks were prepared by inoculating RD cells cultured to approximately 90% confluency in T75 flasks at 33°C and 5% CO_2 at an MOI of 0.01 in Infection Media (IM). Once cytopathic effect was evident (3-5 days) lysates were collected by three freeze-thaw cycles. Titering was performed by methylcellulose plaque assay. RD cells were plated in 6-well tissue culture plates and grown to confluency. A ten-fold dilution series of each viral sample was prepared in IM. RD cells were washed with PBS+ and the viral dilutions were added in a volume of 250µl/well and then placed in the 33°C incubator for one hour with gentle rocking every 15 minutes. The viral inoculum was aspirated, 2mL of 1% methylcellulose in MEM was added to each well as an overlay medium, and the plates were returned to the 33°C incubator for 3 days. To fix and harvest the plates, 2 mL of 10% neutral buffered formalin (VWR, 10015-194) was added dropwise and incubated overnight at room temperature. The formalin/cellulose mixture was swirled and decanted off, and then the cells were stained with naphthol blue black (Millipore Sigma) overnight and washed with water. Plaques were counted manually in a well containing 30-100 plaques, and pfu/ml was calculated by (number of plaques) / (0.25 mL) x (dilution factor).

Cell lines and induced pluripotent stem cells

RD cells, HEK293T cells, and HeLa cells were from ATCC (CCL-136, CRL-3216, and CRM-CCL-2, respectively). iPSC lines were from the Cedars Sinai Biomanufacturing Center repository, and included lines CS0002, CS0003, CS88, CS0YX7, and CS8VTR. iPSCs were maintained in Essential 8 Flex media (Thermo Fisher) on 6-well tissue culture plates coated with Cultrex UltiMatrix Reduced Growth Factor Basement Membrane Extract (R&D Systems BME001), manually cleaned to remove differentiated cells, and passaged as colonies using ReLeSR passaging reagent (STEMCELL Technologies). Motor neuron differentiation was performed following the direct-induced motor neurons (diMN) protocol reported previously (NeuroLINCS Consortium et al. 2021). In brief, iPSCs were grown to 30-40% confluency and then fed daily with S1 media for 6 days for neuroepithelial induction. On day 6, neuroepithelial cells were collected following incubation with Accutase (Millipore Sigma), using gentle pipetting to release cells from the centers of the colonies. Neuroepithelial cells were triturated to a single cell suspension and then collected by centrifugation at 200*g*. These cells were cryopreserved using Cryostor (STEMCELL Technologies) for storage in liquid nitrogen until later use. Day 6 neuroepithelial cells were thawed and replated into UltiMatrix-coated tissue culture dishes in S2 media with ROCK inhibitor Y-27632 (Cayman Chemical) at 20µM, and then fed daily on days 7-12 with S2 without ROCK inhibitor. This stage generates motor neuron precursor cells. On day 12, motor neuron precursors were collected as a single cell suspension with 0.05% Trypsin and replated onto the desired format for each

experiment. Where indicated, nucleofection was performed at this step, prior to replating. From day 12 onward, cells were fed with S3 media to promote terminal maturation and maintenance of motor neurons. The diMN protocol produces cultures containing approximately 80% Tuj1^{+} neurons, including 40% Islet-1^{+} mature motor neurons and 40% Nkx6.1^{+} immature motor neurons (NeuroLINCS Consortium et al. 2021).

Western blotting

Cells were harvested by scraping in ice-cold PBS, pelleted by centrifugation at 500*g* for 5 minutes at 4°C, and PBS was aspirated off. Lysis was achieved by resuspension in ice-cold RIPA buffer (Millipore Sigma) supplemented with cOmplete protease inhibitor cocktail (Millipore Sigma) followed by sonication. Protein concentrations were measured by DC protein assay (Bio-Rad). Samples were prepared by diluting a constant protein quantity by mass with deionized water and 4X Laemmli buffer (Bio-Rad) to a final concentration of 1X. Protein electrophoresis was performed in Bio-Rad Criterion Stain-Free gels and then transferred onto low-fluorescence PVDF membranes using the Transblot Turbo system (Bio-Rad). Total protein stain for confirmation of proper transfer and normalization of quantitative data was by Ponceau S stain (Bio-Rad; Figures 1A-B) or by stain-free imaging (Figures 1C-D, S1). Blots were blocked in 5% non-fat milk in TBS with 0.1% Tween-20 (TBS-T) for 1 hour. Primary antibodies were applied in TBS-T overnight at 4°C. Blots were then washed three times in TBS-T and incubated for one hour in secondary antibody at a concentration of 1:20,000. Blots were washed three more times with TBS-T, twice with TBS, and then developed using SuperSignal West Atto ECL substrate (Thermo Fisher). Images were acquired using a GE Healthcare ImageQuant LAS 4000 (Figures 1A-B) or Bio-Rad ChemiDoc MP Imaging System (Figures 1C-D, S1). Quantification of western blot images was performed using ImageJ software and normalized to the total protein stain.

Recombinant Enterovirus D68 proteases

Recombinant proteases were produced based on the sequence of US/MO/2014-18947. 3C^{pro} was produced by Biomatik. 2A^{pro} produced by standard methods did not demonstrate evidence of protease activity. We therefore generated a SUMO-2A^{pro} fusion protein, based on a strategy previously reported to circumvent this technical limitation thought to be due to improper folding (Musharrafieh et al. 2019). The sequence of 2A^{pro} was codon-optimized for E. coli using the IDT codon optimization tool (*https://www.idtdna.com/pages/tools/codon-optimization-tool*) and generated as synthetic DNA (Integrated DNA Technologies) for In-Fusion Snap Assembly into the peSUMOstar plasmid as detailed above to encode His$_6$-SUMO-2A^{pro}. BL21(DE3) competent cells (New England BioLabs) were transformed with peSUMOstar-2A^{pro}, grown in a shaker-incubator at 37°C in the presence of kanamycin 50µg/mL to an optical density of 0.6-0.75, cooled to 18°C, and then protein expression was induced with 0.5mM IPTG for 24 hours. Cells were harvested by centrifugation at 3500*g* for 20 minutes. The cell pellet with resuspended and lysed in 50mM sodium phosphate, 300 mM sodium chloride, 10nM imidazole, 1mg/mL lysozyme (Roche), and 3 units/mL Benzonase nuclease (Millipore Sigma) at pH 8.0 and incubated on ice for 30 minutes. The lysate was loaded onto Ni-NTA spin columns (Qiagen) and washed with a buffer containing 50mM sodium phosphate, 300 mM sodium chloride, and 20nM imidazole at pH 8.0, then eluted with a buffer containing 50mM sodium phosphate, 300 mM sodium chloride, and 500nM imidazole at pH 8.0.

Recombinant protease digestion assay

To generate a substrate enriched for nucleoporins, a nuclear lysate was collected from HEK293T cells using the NE-PER extraction kit (Thermo Fisher). Nuclear lysates and recombinant proteases were dialyzed overnight at 4°C into reaction buffer (20 mM HEPES pH 7.4, 150 mM potassium acetate, and 1 mM DTT). Lysates were diluted to a concentration of 1µg/µL in reaction buffer with proteases added at a ratio (protease:lysate by mass) of 1:50 for SUMO-2A^{pro} and 1:200 for 3C^{pro}. Proteases were omitted in the case of negative control samples. The samples were incubated at

37°C with rotation at 300rpm for the indicated times. The reaction was stopped via the addition of 4X Laemmli buffer to a final concentration of 1X, followed by incubation for 5 minutes at 100°C. Samples were analyzed by Western blotting.

Nucleocytoplasmic transport assays

HeLa cells or RD cells were plated onto UltiMatrix-coated 96-well glass-bottom plates (Cellvis), cultured in Complete Media, and transfected on day 1 with a reporter construct (NLS-tdTomato, NLS-tdTomato-NES, tdTomato-NES, mCherry-LINus, NLS-mCherry-LEXY) and the nuclear marker H2A-iRFP670. On day 2, they were transfected with the protease-containing vector or empty vector control, or infected with EV-D68 mock-infected. Imaging was completed at the indicated number of hours after the second transfection or infection on a Molecular Devices ImageXpress Confocal high content imaging system. For photoinducible reporters (mCherry-LINus and NLS-mCherry-LEXY), images were acquired every 15 seconds, each beginning with a 1-second pulse of the 488nm laser at maximum intensity to maintain the reporter in its activated state. Image analysis was performed in automated fashion using MetaXpress software (Molecular Devices). A custom analysis protocol was developed to select only GFP^+ cells with size and morphology typical of live cells, to define the area of the nucleus using the H2A-iRFP670 signal, exclude nuclei with a condensed or mitotic morphology, and to define the perinuclear cytoplasm as a concentric ring outside of the nucleus. The average intensity of the reporter signal in the nucleus and perinuclear cytoplasm were measured and reported as Log_2 of the nucleus/cytoplasm ratio. Cells were excluded from the analysis when the intensity of the reporter signal was too low to be distinguished from background or high enough to create shine-through artefact in the green channel, up to a maximum of 50% of the pixel depth of the image to ensure signal in the linear range. Due to inherent variability in signal intensity, these minimum and maximum intensity values were determined empirically for each independent biological replicate.

For assays in diMN, cells were nucleofected with hMAP2-pGreenZero, MAP2-H2A-iRFP670, and the reporter construct on day 12 of differentiation and plated to UltiMatrix-coated 96-well glass-bottom plates at a density of 2.5×10^5 cells/well. On day 18, they were infected with EV-D68 at an MOI of 2.5. Imaging was performed at 24 hours post-infection. Analysis was as above, except that the perinuclear cytoplasm was defined as the intersection between the cytoplasmic GFP signal and a concentric ring outside the nucleus.

Dextran exclusion assay

Digitonin permeabilization was carried out as previously described (Hayes et al. 2020) with some adjustments. Briefly, HeLa cells were seeded onto a UltiMatrix-coated 96-well glass-bottom plate (Cellvis) and maintained in Complete Media. Cells were transfected 15 hours before imaging at 60-70% confluency with bicistronic reporter constructs encoding a nuclear marker and the protease of interest or empty vector (pLenti-IRES-H2A-iRFP, pLenti-IRES-H2A-iRFP(P2A)2Apro, or pLenti-IRES-H2A-iRFP(P2A)3Cpro). To permeabilize, cells were kept on ice and washed with ice-cold PBS for 5 minutes. Digitonin was added at varying concentrations for 10 minutes in permeabilization buffer (PB; 20 mM HEPES, 110 mM KOAc, 5 mM Mg(OAc)2, 0.5 mM EGTA, 250 mM sucrose) to identify the concentration that permeabilized the plasma membrane while leaving the nuclear envelope intact. The optimized digitonin concentration varied depending on the cell density, but the same concentration was used across each biological replicate, with 30-40 µg/mL being used for analysis. Permeabilized cells were washed twice for 5 minutes with modified transport buffer (TRB; 20 mM HEPES, 110 mM KOAc, 2 mM Mg(OAc)2, 5 mM NaOAc, 0.5 mM EGTA, 250 mM sucrose). Cells were kept in TRB with Hoechst (5 µg/mL) on ice until imaging.

Imaging was performed on a Zeiss LSM880 Airyscan confocal microscope and processed using ImageJ. FITC-conjugated 70kDa dextran (Millipore Sigma) was diluted in TRB and added to each well immediately before imaging at a final concentration of 0.6 mg/mL. Images were acquired every 30 seconds for 5 minutes. For each field, cells were analyzed only if the nuclei expressed H2A-iRFP670, had intact and visible nuclear membranes, were regularly shaped, and had clear and sharp boundaries between the nucleus and the cytoplasm. Images were excluded if a majority

of the cells in the field were permeabilized regardless of transfection status, indicating general over-permeabilization. Cells were also excluded if they were impermeabilized (indicated by the absence of a visible nuclear membrane), if nuclei were not completely within the plane of imaging, or if there was drift of the focal plane during time course imaging. Data were reported as the average FITC intensity in the nucleus divided by the average FITC intensity of the extracellular background.

Propidium iodide viability assay

HeLa cells were transfected as in the nucleocytoplasmic transport assays, except omitting the reporter construct. Staurosporine 2 μM was added to the positive control group two hours before propidium iodide as a positive control. Propidium iodide 100μg/mL was added to all groups 20 hours post-transfection and 15 minutes prior to imaging. Image acquisition and analysis was the same as for the nucleocytoplasmic transport assays, selecting only GFP+ cells with normal size and morphology. Instead of calculating the nuclear-cytoplasmic ratio of signal in the red channel, the intensity of signal in the nucleus was recorded. To determine the minimum intensity cutoff for propidium iodide positivity, histograms were plotted for signal intensity in the staurosporine-treated group, and a cutoff for positive cells was determined by identifying the inflection point in the biphasic distribution.

Poly-A FISH

HeLa cells were plated on UltiMatrix-coated 96-well glass-bottom plates (Cellvis) and transfected with pLenti-IRES-GFP, pLenti-IRES-GFP-2A^{pro}, or pLenti-IRES-GFP-3C^{pro}. Twenty hours later, they were washed with PBS, fixed for 30 minutes in 4% paraformaldehyde, washed two more times with PBS, then incubated 10 min each with ice-cold 100% methanol followed by 100% ethanol. Cells were incubated with 1ng/μL of Cy3-oligo-dT (Genelink) in hybridization buffer (30μM sodium citrate, 300μM sodium chloride, 10% formamide, 10% dextran sulfate, 50μg yeast tRNA (Millipore Sigma) in DEPC-treated water for 1 hour at 37°C. To enhance the GFP signal, the cells were then immunofluorescently stained for GFP. Cells were washed with PBS and then blocked in blocking solution (5% goat serum, 1% bovine serum albumin in PBS) for one hour at room temperature and then incubated in primary antibody against GFP diluted 1:200 in 1/4x blocking solution overnight at 4°C. The cells were then washed twice with PBS and then incubated with AlexaFluor488-conjugated secondary antibody for 1 hour in 1/4x blocking solution. Finally, the cells were washed with PBS, counterstained with Hoechst 33342 nuclear stain (Cell Signaling) at 5μg/mL for 15 minutes, and then mounted with PBS glycerol for imaging. Imaging was performed and analyzed on a Molecular Devices ImageXpress Confocal high content imaging system as described above for NCT assays.

5-Ethinyl Uridine pulse-chase

HEK293T cells were plated on UltiMatrix-coated 96-well glass-bottom plates (Cellvis) and transfected with pLenti-IRES-GFP, pLenti-IRES-GFP-2A^{pro}, or pLenti-IRES-GFP-3C^{pro}. Twenty hours after transfection, the cell culture medium was replaced with fresh media containing 1mM 5-ethinyl uridine (EU; Vector Laboratories) for a 1-hour pulse to label nascent RNA. To preferentially label the products of each RNA polymerase, inhibitors of the other two RNA polymerases were included during the EU pulse. These were 0.05ng/mL actinomycin D, 0.05 ng/ml α-amanitin, and 50 μM CAS 577784-91-9 to inhibit RNA polymerases I, II, and III, respectively. The EU-containing media was aspirated off, washed once with PBS, and then chased with fresh Complete Media for 0, 2, 4, or 8 hours. For RD cells, the cells were infected with EV-D68 at MOI5 and the pulse-chase labeling was begun 24 hours after infection, with the chase being completed at 0, 1, 2, or 4 hours after the end of the pulse. Cells were collected by fixation with 3% paraformaldehyde for 15 minutes, washed twice with PBS, and then permeabilized with 0.5% Triton-X100 for 15 minutes. EU was fluorescently labeled with AZDye594-azide via click chemistry using the Click&Go cell reaction kit following the manufacturer's instructions (Vector Laboratories). The cells were immunofluorescently co-stained for GFP and counterstained with Hoechst 33342 as described

above for the poly-A-FISH assay. Imaging and analysis was likewise performed as above, except nuclear signal intensity of the EU stain was reported instead of nuclear/cytoplasmic ratio, because the cytoplasmic signal was not consistently distinguishable from background. Intensities were normalized such that the intensity at t=0 was considered 100%.

Motor neuron toxicity

Day 12 diMN precursors were transfected with hMAP2-pGreenZero using a Lonza Nucleofector 4D X unit, with the P3 primary cell kit on program DC-104. Cells were replated into UltiMatrix-coated 96-well glass bottom plates at a density of 100,000 cells/well in S3 media with 20μM Y-27632. After 24 hours, the cells were re-fed without Y-27632 and maintained in S3 media until day 32 of differentiation. These diMNs were infected with EV-D68 at MOI 5 in Infection Media for one hour at 37°C with rocking every 15 minutes, then fed with S3 media. diMNs were imaged on a Molecular Devices ImageXpress Confocal high content imaging system immediately following infection (considered t=0) and then once daily for four additional days. GFP^+ neurons were counted via automated image analysis in MetaXpress software.

Growth curves on motor neurons

Day 12 diMN precursors were plated onto UltiMatrix-coated 96-well plastic tissue culture plates at a density of 75,000 cells/well and maintained in S3 media until day 32 of differentiation. diMNs were infected with EV-D68 at MOI 0.5 as described above. Virus was collected at the indicated times by subjecting the plates to three freeze-thaw cycles. Viral titers were measured by methylcellulose plaque assay.

Statistics

Statistical analyses and preparation of graphs were performed in GraphPad Prism 10 software. Statistical methods for each experiment are described in the corresponding figure legend.

Supplementary data

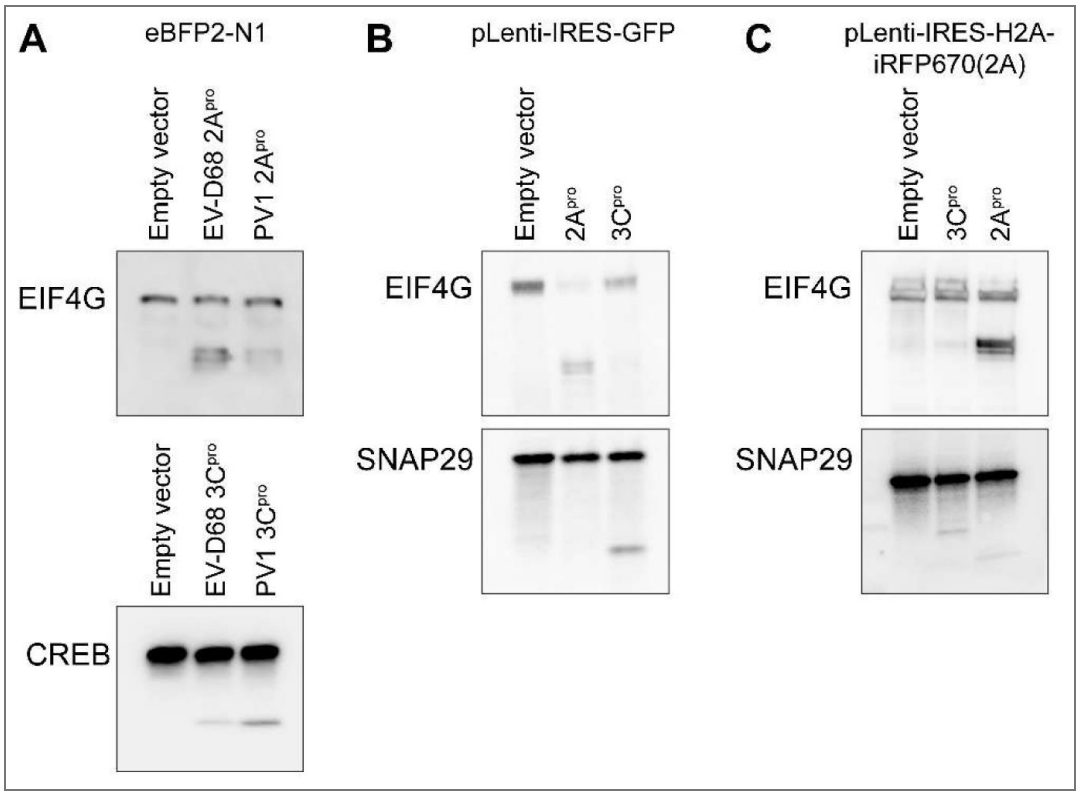

Figure S1. **Western blots demonstrating evidence of $2A^{pro}$ and $3C^{pro}$ protease activity on well-established substrates following transfection with each of the expression vectors used in this study.**

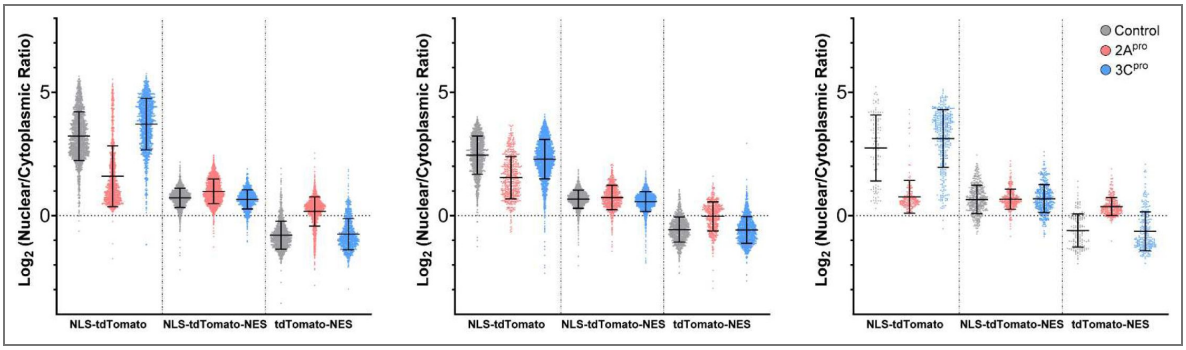

Figure S2. Source data for Figure 2A, showing individual cell level data for three independent replicates.

Bars are mean ± S.D.

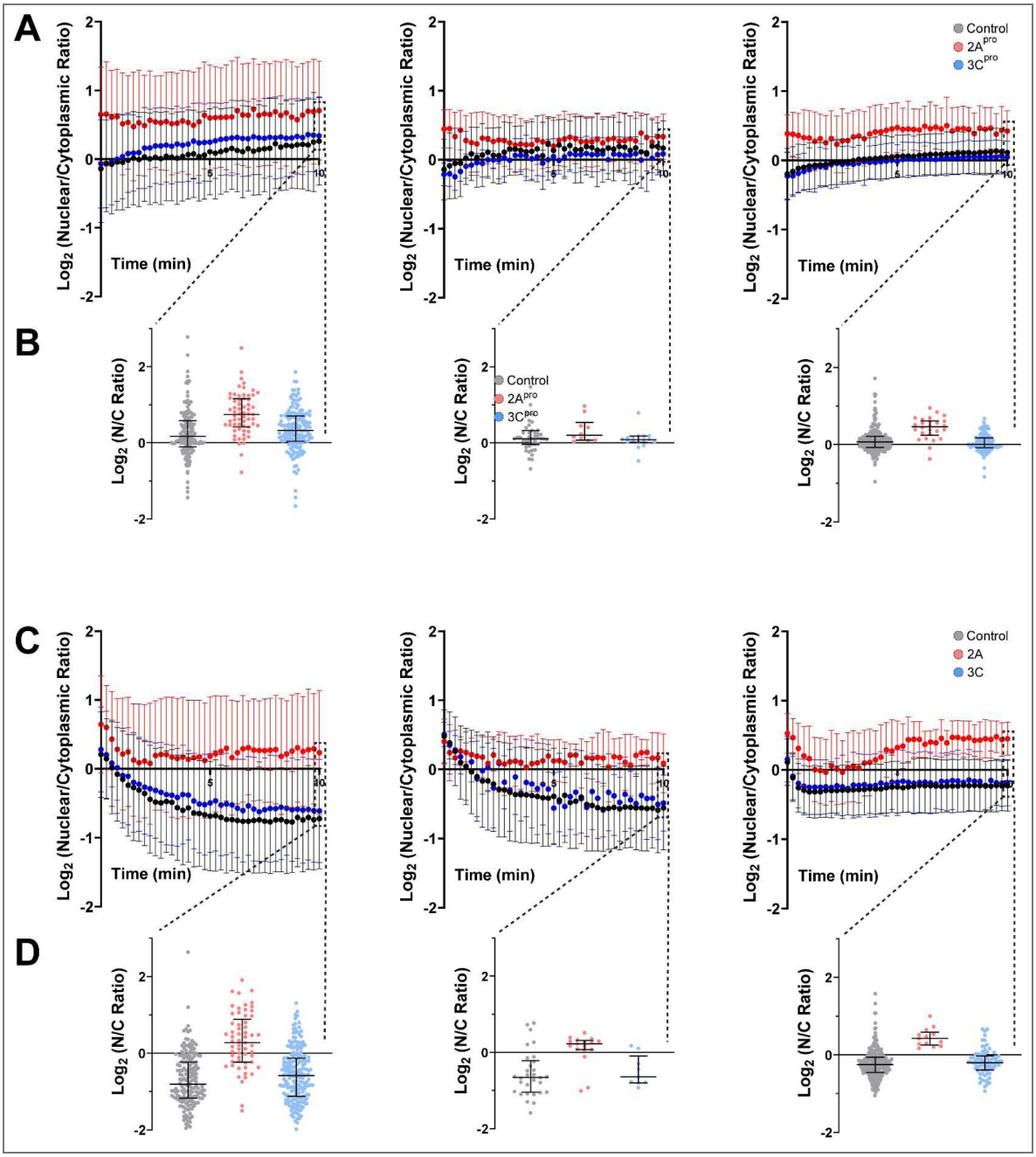

Figure S3. Source data for Figure 2D, showing mean ± S.D. values from three independent replicates for LINus (A) and LEXY (C) nucleocytoplasmic transport reporters.

Individual cell level data is also presented at t=10 min for LINus (B) and LEXY (D). Bars are mean ± S.D.

Figure S4. Source data for Figure 3A, demonstrating individual cell-level data across four independent replicates.

Bars are mean ± S.D.

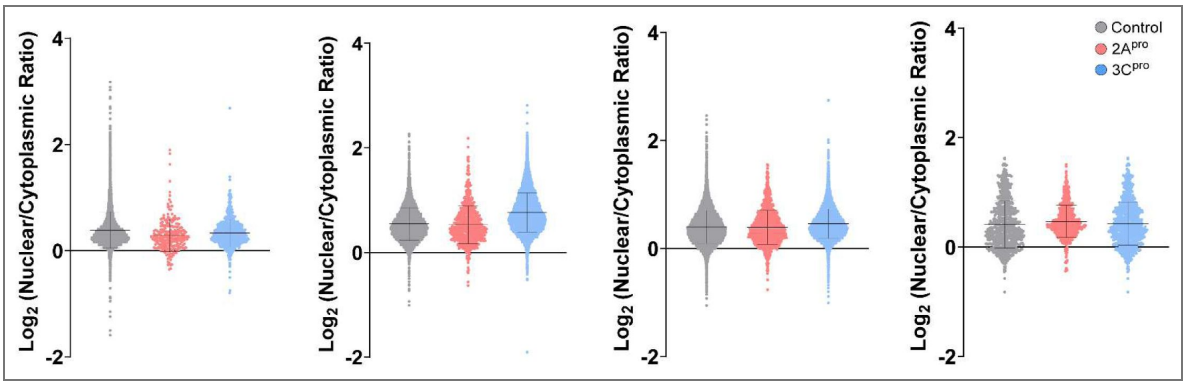

Figure S5. Source data for figures 4C (A) and 4D (B), showing individual cell-level data for three independent replicates in diMNs derived from iPSC lines CS0002, CS0003, and CS88.

Bars are mean ± S.D.

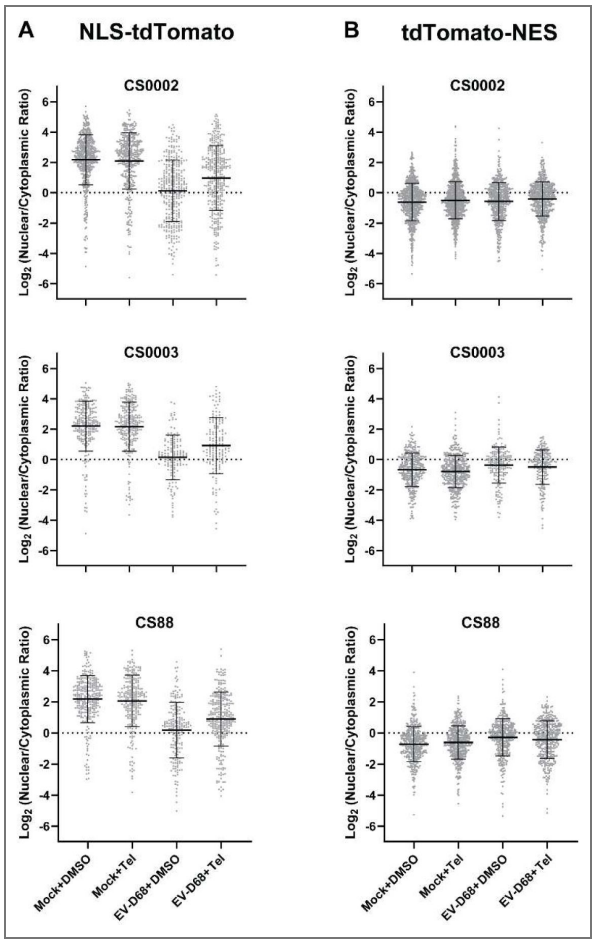

Data availability

Source data for all figures and original uncropped Western blots are being deposited in the Johns Hopkins Data Repository and are uploaded along with this submission as a supplemental file ("Raw data and uncropped western blots.zip"). No large datasets were generated.

Acknowledgements

We thank Dr. Andrew Pekosz for helpful discussions and the gift of US/MD/2018-23209. We thank Lin Jin, Lin Xue, and Kelly Bowen for technical expertise. The following reagent was obtained through BEI Resources, NIAID, NIH: Enterovirus Species D Type 68, US/MO/14-18947 (produced in serum-free A549 cells), NR-52013. This work was supported by the National Institutes of Health (5K 12NS098482, K08 NS124989, R01 NS143998 and P50 HD103538).

Additional information

Funding

Funder	Grant reference number	Author
HHS | NIH | National Institute of Neurological Disorders and Stroke (NINDS)	5K12NS098482	Matthew J Elrick
HHS | NIH | National Institute of Neurological Disorders and Stroke (NINDS)	K08NS124989	Matthew J Elrick
HHS | NIH | National Institute of Neurological Disorders and Stroke (NINDS)	R01NS143998	Matthew J Elrick
HHS | NIH | Eunice Kennedy Shriver National Institute of Child Health and Human Development (NICHD)	P50HD103538	Matthew J Elrick

Author ORCID iDs

Michael T Imai: https://orcid.org/0009-0000-0354-4095
Matthew J Elrick: https://orcid.org/0000-0001-7608-7593

References

Adam S. A., Marr R. S., Gerace L. (1990) Nuclear protein import in permeabilized mammalian cells requires soluble cytoplasmic factors. *J Cell Biol* **111**:807-816 https://doi.org/10.1083/jcb.111.3.807 | PubMed

Addis R. C., Hsu F. C., Wright R. L., Dichter M. A., Coulter D. A., Gearhart J. D. (2011) Efficient conversion of astrocytes to functional midbrain dopaminergic neurons using a single polycistronic vector. *PLoS One* **6**:e28719 https://doi.org/10.1371/journal.pone.0028719 | PubMed

Back S. H., Kim Y. K., Kim W. J., Cho S., Oh H. R., Kim J. E., Jang S. K. (2002) Translation of polioviral mRNA is inhibited by cleavage of polypyrimidine tract-binding proteins executed by polioviral 3C(pro). *J Virol* **76**:2529-2542 https://doi.org/10.1128/jvi.76.5.2529-2542.2002 | PubMed

Baskerville V., Rapuri S., Mehlhop E., Coyne A. N. (2024) SUN1 facilitates CHMP7 nuclear influx and injury cascades in sporadic amyotrophic lateral sclerosis. *Brain* **147**:109-121 https://doi.org/10.1093/brain/awad291 | PubMed

Belov G. A., Evstafieva A. G., Rubtsov Y. P., Mikitas O. V., Vartapetian A. B., Agol V. I. (2000) Early alteration of nucleocytoplasmic traffic induced by some RNA viruses. *Virology* **275**:244-248 https://doi.org/10.1006/viro.2000.0427 | PubMed

Belov G. A., Lidsky P. V., Mikitas O. V., Egger D., Lukyanov K. A., Bienz K., Agol V. I. (2004) Bidirectional Increase in Permeability of Nuclear Envelope upon Poliovirus Infection and Accompanying Alterations of Nuclear Pores. *Journal of Virology* **78**:10166-10177 https://doi.org/10.1128/jvi.78.18.10166-10177.2004 | PubMed

Brown D. M., Hixon A. M., Oldfield L. M., Zhang Y., Novotny M., Wang W., Das S. R., Shabman R. S., Tyler K. L., Scheuermann R. H. (2018) Contemporary Circulating Enterovirus D68 Strains Have Acquired the Capacity for Viral Entry and Replication in Human Neuronal Cells. *Mbio* **9** https://doi.org/10.1128/mbio.01954-18 | PubMed

Castello A., Alvarez E., Carrasco L. (2006) Differential cleavage of eIF4GI and eIF4GII in mammalian cells. Effects on translation. *J Biol Chem* **281**:33206-33216 https://doi.org/10.1074/jbc.m604340200 | PubMed

Castello A., Izquierdo J. M., Welnowska E., Carrasco L. (2009) RNA nuclear export is blocked by poliovirus 2A protease and is concomitant with nucleoporin cleavage. *Journal of Cell Science* **122**:3799-3809 https://doi.org/10.1242/jcs.055988 | PubMed

Consortium N., Li J., Lim R. G., Kaye J. A., Dardov V., Coyne A. N., Wu J., Milani P., Cheng A., Thompson T. G., *et al.* (2021) An integrated multi-omic analysis of iPSC-derived motor neurons from C9ORF72 ALS patients. *iScience* **24**:103221 https://doi.org/10.1016/j.isci.2021.103221 | PubMed

Coyne A. N., Baskerville V., Zaepfel B. L., Dickson D. W., Rigo F., Bennett F., Lusk C. P., Rothstein J. D. (2021) Nuclear accumulation of CHMP7 initiates nuclear pore complex injury and subsequent TDP-43 dysfunction in sporadic and familial ALS. *Science Translational Medicine* **13**:eabe1923 https://doi.org/10.1126/scitranslmed.abe1923 | PubMed

Coyne A. N., Rothstein J. D. (2021) The ESCRT-III protein VPS4, but not CHMP4B or CHMP2B, is pathologically increased in familial and sporadic ALS neuronal nuclei. *Acta Neuropathologica Communications* **9** https://doi.org/10.1186/s40478-021-01228-0 | PubMed

Coyne A. N., Zaepfel B. L., Hayes L., Fitchman B., Salzberg Y., Luo E. C., Bowen K., Trost H., Aigner S., Rigo F., *et al.* (2020) G4C2 Repeat RNA Initiates a POM121-Mediated Reduction in Specific Nucleoporins in C9orf72 ALS/FTD. *Neuron* **107**:1124-1140 e1111 https://doi.org/10.1016/j.neuron.2020.06.027 | PubMed

Delhaye S., van Pesch V., Michiels T. (2004) The leader protein of Theiler's virus interferes with nucleocytoplasmic trafficking of cellular proteins. *J Virol* **78**:4357-4362 https://doi.org/10.1128/jvi.78.8.4357-4362.2004 | PubMed

Eftekharzadeh B., Daigle J. G., Kapinos L. E., Coyne A., Schiantarelli J., Carlomagno Y., Cook C., Miller S. J., Dujardin S., Amaral A. S., *et al.* (2018) Tau Protein Disrupts Nucleocytoplasmic Transport in Alzheimer's Disease. *Neuron* **99**:925-940 e927 https://doi.org/10.1016/j.neuron.2018.07.039 | PubMed

Elrick M. J., Pekosz A., Duggal P. (2021) Enterovirus D68 Molecular and Cellular Biology, and Pathogenesis. *J Biol Chem* 100317 https://doi.org/10.1016/j.jbc.2021.100317 | PubMed

Freibaum B. D., Lu Y., Lopez-Gonzalez R., Kim N. C., Almeida S., Lee K. H., Badders N., Valentine M., Miller B. L., Wong P. C., *et al.* (2015) GGGGCC repeat expansion in C9orf72 compromises nucleocytoplasmic transport. *Nature* **525**:129-133 https://doi.org/10.1038/nature14974 | PubMed

Frost J., Rudy M. J., Leser J. S., Tan H., Hu Y., Wang J., Clarke P., Tyler K. L. (2023) Telaprevir Treatment Reduces Paralysis in a Mouse Model of Enterovirus D68 Acute Flaccid Myelitis. *J Virol* **97**:e0015623 https://doi.org/10.1128/jvi.00156-23 | PubMed

Ghildyal R., Jordan B., Li D., Dagher H., Bardin P. G., Gern J. E., Jans D. A. (2009) Rhinovirus 3C protease can localize in the nucleus and alter active and passive nucleocytoplasmic transport. *J Virol* **83**:7349-7352 https://doi.org/10.1128/jvi.01748-08 | PubMed

Goedhart J., von Stetten D., Noirclerc-Savoye M., Lelimousin M., Joosen L., Hink M. A., van Weeren L., Gadella T. W., Royant A. (2012) Structure-guided evolution of cyan fluorescent proteins towards a quantum yield of 93%. *Nat Commun* **3**:751 https://doi.org/10.1038/ncomms1738 | PubMed

Grima J. C., Daigle J. G., Arbez N., Cunningham K. C., Zhang K., Ochaba J., Geater C., Morozko E., Stocksdale J., Glatzer J. C., *et al.* (2017) Mutant Huntingtin Disrupts the Nuclear Pore Complex. *Neuron* **94**:93-107 e106 https://doi.org/10.1016/j.neuron.2017.03.023 | PubMed

Gustin K. E., Sarnow P. (2001) Effects of poliovirus infection on nucleo-cytoplasmic trafficking and nuclear pore complex composition. *EMBO J* **20**:240-249 https://doi.org/10.1093/emboj/20.1.240 | PubMed

Gustin K. E., Sarnow P. (2002) Inhibition of nuclear import and alteration of nuclear pore complex composition by rhinovirus. *J Virol* **76**:8787-8796 https://doi.org/10.1128/jvi.76.17.8787-8796.2002 | PubMed

Hayes L. R., Duan L., Bowen K., Kalab P., Rothstein J. D. (2020) C9orf72 arginine-rich dipeptide repeat proteins disrupt karyopherin-mediated nuclear import. *eLife* **9** https://doi.org/10.7554/elife.51685 | PubMed

Hixon A. M., Clarke P., Tyler K. L. (2019) Contemporary Circulating Enterovirus D68 Strains Infect and Undergo Retrograde Axonal Transport in Spinal Motor Neurons Independent of Sialic Acid. *J Virol* **93**:e00578-00519 https://doi.org/10.1128/jvi.00578-19 | PubMed

Hixon A. M., Yu G., Leser J. S., Yagi S., Clarke P., Chiu C. Y., Tyler K. L. (2017) A mouse model of paralytic myelitis caused by enterovirus D68. *PLoS Pathog* **13**:e1006199 https://doi.org/10.1371/journal.ppat.1006199 | PubMed

Jovicic A., Mertens J., Boeynaems S., Bogaert E., Chai N., Yamada S. B., Paul J. W., Sun S., Herdy J. R., Bieri G., *et al.* (2015) Modifiers of C9orf72 dipeptide repeat toxicity connect nucleocytoplasmic transport defects to FTD/ALS. *Nat Neurosci* **18**:1226-1229 https://doi.org/10.1038/nn.4085 | PubMed

Juhlen R., Fahrenkrog B. (2018) Moonlighting nuclear pore proteins: tissue-specific nucleoporin function in health and disease. *Histochem Cell Biol* https://doi.org/10.1007/s00418-018-1748-8 | PubMed

Krull S., Dörries J., Boysen B., Reidenbach S., Magnius L., Norder H., Thyberg J., Cordes V. C. (2010) Protein Tpr is required for establishing nuclear pore-associated zones of heterochromatin exclusion. *The EMBO Journal* **29**:1659-1673 https://doi.org/10.1038/emboj.2010.54 | PubMed

Lenart P., Ellenberg J. (2006) Monitoring the permeability of the nuclear envelope during the cell cycle. *Methods* **38**:17-24 https://doi.org/10.1016/j.ymeth.2005.07.010 | PubMed

Lin D. H., Hoelz A. (2019) The Structure of the Nuclear Pore Complex (An Update). *Annu Rev Biochem* https://doi.org/10.1146/annurev-biochem-062917-011901 | PubMed

Liu Y., Sheng J., Baggen J., Meng G., Xiao C., Thibaut H. J., van Kuppeveld F. J., Rossmann M. G. (2015) Sialic acid-dependent cell entry of human enterovirus D68. *Nat Commun* **6**:8865 https://doi.org/10.1038/ncomms9865 | PubMed

Lizcano-Perret B., Michiels T. (2021) Nucleocytoplasmic Trafficking Perturbation Induced by Picornaviruses. *Viruses* **13**:1210 https://doi.org/10.3390/v13071210 | PubMed

McBride A. E., Schlegel A., Kirkegaard K. (1996) Human protein Sam68 relocalization and interaction with poliovirus RNA polymerase in infected cells. *Proc Natl Acad Sci U S A* **93**:2296-2301 https://doi.org/10.1073/pnas.93.6.2296 | PubMed

Meerovitch K., Svitkin Y. V., Lee H. S., Lejbkowicz F., Kenan D. J., Chan E. K., Agol V. I., Keene J. D., Sonenberg N. (1993) La autoantigen enhances and corrects aberrant translation of poliovirus RNA in reticulocyte lysate. *J Virol* **67**:3798-3807 https://doi.org/10.1128/jvi.67.7.3798-3807.1993 | PubMed

Musharrafieh R., Ma C., Zhang J., Hu Y., Diesing J. M., Marty M. T., Wang J. (2019) Validating Enterovirus D68-2A(pro) as an Antiviral Drug Target and the Discovery of Telaprevir as a Potent D68-2A(pro) Inhibitor. *J Virol* **93** https://doi.org/10.1128/jvi.02221-18 | PubMed

Niopek D., Benzinger D., Roensch J., Draebing T., Wehler P., Eils R., Di Ventura B. (2014) Engineering light-inducible nuclear localization signals for precise spatiotemporal control of protein dynamics in living cells. *Nature Communications* **5** https://doi.org/10.1038/ncomms5404 | PubMed

Niopek D., Wehler P., Roensch J., Eils R., Di Ventura B. (2016) Optogenetic control of nuclear protein export. *Nature Communications* **7**:10624 https://doi.org/10.1038/ncomms10624 | PubMed

Oberste M. S., Maher K., Schnurr D., Flemister M. R., Lovchik J. C., Peters H., Sessions W., Kirk C., Chatterjee N., Fuller S., *et al.* (2004) Enterovirus 68 is associated with respiratory illness and shares biological features with both the enteroviruses and the rhinoviruses. *J Gen Virol* **85**:2577-2584 https://doi.org/10.1099/vir.0.79925-0 | PubMed

Park N., Katikaneni P., Skern T., Gustin K. E. (2008) Differential targeting of nuclear pore complex proteins in poliovirus-infected cells. *J Virol* **82**:1647-1655 https://doi.org/10.1128/jvi.01670-07 | PubMed

Park N., Schweers N. J., Gustin K. E. (2015) Selective Removal of FG Repeat Domains from the Nuclear Pore Complex by Enterovirus 2A(pro). *J Virol* **89**:11069-11079 https://doi.org/10.1128/jvi.00956-15 | PubMed

Park N., Skern T., Gustin K. E. (2010) Specific cleavage of the nuclear pore complex protein Nup62 by a viral protease. *J Biol Chem* **285**:28796-28805 https://doi.org/10.1074/jbc.m110.143404 | PubMed

Rousseaux M. W., de Haro M., Lasagna-Reeves C. A., De Maio A., Park J., Jafar-Nejad P., Al-Ramahi I., Sharma A., See L., Lu N., *et al.* (2016) TRIM28 regulates the nuclear accumulation and toxicity of both alpha-synuclein and tau. *eLife* **5** https://doi.org/10.7554/elife.19809 | PubMed

Serganov A. A., Udi Y., Stein M. E., Patel V., Fridy P. C., Rice C. M., Saeed M., Jacobs E. Y., Chait B. T., Rout M. P. (2022) Proteomic elucidation of the targets and primary functions of the picornavirus 2A protease. *J Biol Chem* **101882** https://doi.org/10.1016/j.jbc.2022.101882 | PubMed

Shani V., Safory H., Szargel R., Wang N., Cohen T., Elghani F. A., Hamza H., Savyon M., Radzishevsky I., Shaulov L., *et al.* (2019) Physiological and pathological roles of LRRK2 in the nuclear envelope integrity. *Hum Mol Genet* **28**:3982-3996 https://doi.org/10.1093/hmg/ddz245 | PubMed

Ventoso I., MacMillan S. E., Hershey J. W., Carrasco L. (1998) Poliovirus 2A proteinase cleaves directly the eIF-4G subunit of eIF-4F complex. *FEBS Lett* **435**:79-83 https://doi.org/10.1016/s0014-5793(98)01027-8 | PubMed

Visser L. J., Langereis M. A., Rabouw H. H., Wahedi M., Muntjewerff E. M., de Groot R. J., van Kuppeveld F. J. M. (2019) Essential Role of Enterovirus 2A Protease in Counteracting Stress Granule Formation and the Induction of Type I Interferon. *J Virol* **93**:e00222-00219 https://doi.org/10.1128/jvi.00222-19 | PubMed

Vogt M. R., Wright P. F., Hickey W. F., De Buysscher T., Boyd K. L., Crowe J. E. (2022) Enterovirus D68 in the Anterior Horn Cells of a Child with Acute Flaccid Myelitis. *N Engl J Med* **386**:2059-2060 https://doi.org/10.1056/nejmc2118155 | PubMed

Watters K., Inankur B., Gardiner J. C., Warrick J., Sherer N. M., Yin J., Palmenberg A. C. (2017) Differential Disruption of Nucleocytoplasmic Trafficking Pathways by Rhinovirus 2A Proteases. *J Virol* **91** https://doi.org/10.1128/jvi.02472-16 | PubMed

Watters K., Palmenberg A. C. (2011) Differential processing of nuclear pore complex proteins by rhinovirus 2A proteases from different species and serotypes. *J Virol* **85**:10874-10883 https://doi.org/10.1128/jvi.00718-11 | PubMed

Yalamanchili P., Datta U., Dasgupta A. (1997) Inhibition of host cell transcription by poliovirus: cleavage of transcription factor CREB by poliovirus-encoded protease 3Cpro. *J Virol* **71**:1220-1226 https://doi.org/10.1128/jvi.71.2.1220-1226.1997 | PubMed

Zhang K., Donnelly C. J., Haeusler A. R., Grima J. C., Machamer J. B., Steinwald P., Daley E. L., Miller S. J., Cunningham K. M., Vidensky S., *et al.* (2015) The C9orf72 repeat expansion disrupts nucleocytoplasmic transport. *Nature* **525**:56-61 https://doi.org/10.1038/nature14973 | PubMed

Peer reviews

Reviewer #1 (Public review):

Summary:

Zinn and colleagues investigated the role of proteases 2A and 3C of enterovirus D68 (EVD68), an emerging pathogen associated with outbreaks of acute flaccid myelitis (AFM), a polio-like disease, on the nucleocytoplasmic trafficking in different systems, including human neurons derived from pluripotent cells. They found that 2A specifically cleaved Nup98 and POM121. Using reporter proteins and RNA synthesis and trafficking assays in cells expressing viral proteases, they showed that 2A induces broad loss of the nuclear pore barrier function, but, surprisingly, the RNA export appears to be minimally affected. Since nucleocytoplasmic trafficking defects are known to be associated with neuropatologies, they propose a hypothesis that 2A-dependent cleavage of nucleoporins in motoneurons underlies the development of EVD68-induced AFM. They further show that a 2A-specific inhibitor increases the survival of human neurons differentiated from stem cells upon EVD68 infection.

Strengths:

Use of multiple methods to investigate the effect of 2A and 3C expression on nucleoporin cleavage and nucleocytoplasmic trafficking.

Comments on revisions:

The following issues remain unresolved:

First, the authors still do not show representative images confirming specific nucleoporin degradation (Fig.1), which is the main focus of the work.

Second, the conclusion that 2A-mediated degradation of the nucleo-cytoplasmic barrier does not affect export of the RNA from the nucleus is not supported by the presented data. The representative images shown in Fig 3C do not have the signal for GFP (like in Fig. 2), and therefore it is impossible to see if those cells indeed express EVD68 proteases.

Moreover, to show RNA export, not only the decrease of nuclear EU signal should be quantified, but also the increase of the cytoplasmic signal. The diminishing of the nuclear staining may not necessarily reflect RNA export, but may well be explained by nuclease activity, all the more relevant in cells expressing 2A, where the nuclear-cytoplasmic barrier is disrupted and cytoplasmic nucleases may enter the nucleus.

The same applies to images in Fig. 3D. There are no markers of infection; moreover, the experiment description indicates that EU labeling began at 24 h post-infection with an MOI of 5, i.e., essentially all cells should have been infected. This is difficult to believe as the replication cycle of most EVD68 strains in HeLa cells is no longer than 12 h, yet the images do not show any signs of CPE, and demonstrate a strong EU signal, inconsistent with the expected inhibition of nuclear transcription, a known attribute of enterovirus infections.

The claim that nuclear transcription and RNA export remain unaffected in conditions of 2A-mediated disruption of the nucleo-cytoplasmic barrier is very strong and requires equally strong evidence.

https://doi.org/10.7554/eLife.108672.2.sa3

Reviewer #2 (Public review):

Summary:

This manuscript investigates the role of EV-D68 proteases 2A and 3C in nuclear pore complex (NPC) dysfunction and their contribution to motor neuron toxicity. The authors demonstrate that both proteases cleave only a limited number of nucleoporins, with 2A^pro showing the strongest impact by inhibiting nuclear import and export of proteins and disrupting NPC permeability without affecting RNA export. Importantly, treatment with the 2A^pro inhibitor telaprevir reduced neuronal cell death in a dose-dependent manner, achieving neuroprotection at concentrations below those required to inhibit viral replication. The study addresses a relevant mechanism underlying EV-D68-induced neuropathology and explores a potential therapeutic intervention.

https://doi.org/10.7554/eLife.108672.2.sa2

Reviewer #3 (Public review):

Summary:

The author showed expression of the viral proteases 2Apro and 3Cpro of EV-D68, which cleaved specific components of the nuclear pore complex (Nup98 and POM121 by 2Apro), and 2A but not 3C expression altered nuclear import and export. Similar nucleocytoplasmic transport deficits are observed in EV-D68-infected RD cells and iPSC-derived motor neurons (diMNs). 2A inhibitor telaprevir partially rescued the nucleocytoplasmic transport deficits and suppressed neuronal cell death after infection. While it's clear that 2A can cleave NPC proteins and affect nuclear transport, the link to neurotoxicity after EV-D68 infection is less convincing.

This study opens up a very intriguing hypothesis: that EV-D68 2Apro could be directly responsible for motor neuron cell death, mediated by POM121 and possibly Nup98 cleavage, that ultimately results in paralysis known as acute flaccid myelitis. This hypothesis notably does run counter to other published data showing that human neuronal organoids derived from iPSCs can support productive EV-D68 infection for weeks without cell death and that EV-D68-infected mice can have paralysis prevented by depletion of CD8 T cells, still with EV-D68 infection of the spinal cord. However, even if 2Apro is not ultimately responsible for motor neurons dying in human infections, that does not exclude the possibility that cleavage of nups could still disrupt motor neuron function. Notably, most children with AFM have some amount of motor function return after their acute period of paralysis, but most still have some residual paralysis for years to life. It is possible that 2A pro could mediate the acute onset of weakness, while T cells killing neurons could determine the amount of long-term, residual paralysis.

Strengths:

The characterization of nuclear pore complex components that appear to be targets of both poliovirus and EV-D68 proteases is quite thorough and expansive, so this data set alone will be useful for reference to the field. And the process by which the authors narrowed their focus to EV-D68 2Apro reducing Nup98 and POM121 as consequential to both import and export of nuclear cargo but not RNA was technically impressive, thorough, and convincing. As will be detailed below, when the authors move from studying over-expressed proteases in transformed cell lines to studying actual virus infection in both transformed cell lines and iPSC-derived neurons, some of the data only indirectly support their conclusions; however, the quality of the experiments performed is still high. So even if the claim that 2Apro causes neurotoxicity is circumstantial, the data certainly are intriguing and certainly justify further study of the effects of EV-D68 2Apro on the NPC and how this impacts pathogenesis. This is a convincing start to an intriguing line of inquiry.

Comments on revisions:

The authors have returned a stronger revised manuscript, being responsive to most of the combined reviewers' comments. It was especially important to add the clarity and specificity that the data in this manuscript did not establish a direct link for 2Apro causing AFM. The authors have clarified this language adequately, such that it is appropriate to remove the "incomplete" portion of the short assessment as they have requested. Adding in experiments with EV-D68 virus infection to complement their work with recombinant proteases also strengthened their conclusions.

There are still some areas where discrepancies remain, although these are minor and can mostly be acknowledged as limitations of their approach rather than needing more experiments, unless the authors choose to do the additional experiments. To try to make this understandable, I have copied from the rebuttal letter (*) original comment, (**) author's rebuttal, and (***) a reply to the rebuttal:

(*)(2) Telaprevir was able to rescue nucleocytoplasmic transport in RD cells at low concentrations (Figure 4A). It is not shown if this correlates with its antiviral effect in RD cells, or could this correlate with inhibition of 2A cleavage of Nup98 or POM121, which is never measured.

(**) In the aforementioned new experiment in Figure 4A, we have also included a dose-response curve for telaprevir showing its inhibition of POM121 and Nup98 cleavage.

(***) Fig.4A is in diMN not RD cells. The EC50 of telaprevir could be very different in RD cell vs diMNs. This question remains unanswered.

(*) (3) Building off of the prior point, the authors' claim that the neuroprotective effect of telaprevir is independent of its antiviral effect is not well-founded. Figure 4E (neuroprotection) was done with MOI 5, and Figure 4G (virus growth) was MOI 0.5. Telaprevir neuroprotection is not shown at MOI 0.5, nor is the neuroprotective effect correlated with inhibition of 2A cleavage of Nup98 or POM121.

(**) The selection of MOIs for these two experiments was limited by technical considerations. If the viral growth curve were to be performed at MOI 5, it would be confounded by cell death. Further, a low MOI is required in order to allow multiple rounds of infection, and is therefore more sensitive for assaying the effect of telaprevir on viral replication. On the other hand, at MOI 0.5 diMN death is very gradual, and the neuroprotection assay we would have lacked the statistical power to determine whether a rescue of this small magnitude of toxicity is significant. The EC50 of telaprevir is not expected to vary at different MOIs.

(***) This should be discussed in the Discussion as a limitation of the experiment.

(**) We have also now correlated the inhibition of 2Apro cleavage of Nup98 and POM121 with the neuroprotective effect at comparable concentrations of telaprevir, as described above.

(***) Unless you quantify this, my eye disagrees with you. In Fig.4A, cleavage of NUP98 is rescued by 3uM telaprevir, but that does not seem to be the case for POM121.

Additionally, in Fig. 4D, why is only NLS but not NES is impaired in diMN? This should be discussed.

https://doi.org/10.7554/eLife.108672.2.sa1

Author response:

The following is the authors' response to the original reviews.

> ***eLife Assessment***
>
> *This valuable study examines the cleavage of motor neuron nucleoporins by proteases 2A and 3C of enterovirus D68, a pathogen associated with acute flaccid myelitis. The evidence supporting the effects of EV-D68 proteases on nuclear import and export is solid and confirms previous results on the specific targeting of nucleoporins by proteases from other enteroviruses. However, the claim that cleavage of nucleoporins by EV-D68 2A is neurotoxic, though intriguing, is incomplete, as the evidence is largely indirect.*

We appreciate that the reviewers highlighted multiple strengths of manuscript, including its detailed mechanistic dissection of the disrupted composition and function of the nuclear pore complex during EV-D68 infection, the finding that the viral 2A protease is toxic to motor neurons, and that several novel hypotheses on the pathogenesis of acute flaccid myelitis that are raised by our work.

It appears that two independent eLife Assessments were made regarding the strength of evidence in our manuscript. The evidence supporting the impact of EV-D68 proteases on the NPC was felt to be solid.

A second assessment was made as to whether our data support that "the cleavage of nucleoporins by EV-D68 2A is neurotoxic". We would like to clarify that we did not intend to make this second claim in our manuscript and thought that we had been careful not to do so. In response to reviewer and editorial feedback, we have edited the text to improve the clarity on this issue. Although our data show that $2A^{pro}$ is toxic to motor neurons, it cannot yet be determined whether this toxicity is mediated via $2A^{pro}$'s effects on the NPC. That is a logical hypothesis that arises from our manuscript, which we are testing through ongoing work that will require a significant volume of experiments that are outside the scope of the present study. We view this manuscript as an important first step towards a comprehensive understanding of the role of the 2A protease in the pathogenesis of AFM. Please see the response to point # 3 of Reviewer 2 below for a more detailed discussion of this issue and the changes we have made to the text in response. We respectfully request that a judgement on the role of nucleoporin cleavage as the mechanism of neurotoxicity not be included in the eLife Assessment.

Also in response to reviewer feedback that our data was too reliant on the expression of recombinant viral proteins in isolation, we have added additional experiments extending our results into the context of live virus infection of cell lines and motor neurons. We feel that our revised manuscript has been improved as a result of the reviewers' and editor's input, and provides strong support for the following claims: (1) NPC composition and function is disrupted during EV-D68 infection, (2) $2A^{pro}$ is primarily responsible for functional disruption, and (3) $2A^{pro}$ is neurotoxic.

We appreciate your review of this revised manuscript. Detailed responses to each of the reviewers' comments are provided below.

> ***Public Reviews:***
>
> ***Reviewer #1 (Public review):***
>
> *Summary:*
>
> *Zinn and colleagues investigated the role of proteases 2A and 3C of enterovirus D68 (EVD68), an emerging pathogen associated with outbreaks of acute flaccid myelitis (AFM), a polio-like disease, on the nucleocytoplasmic trafficking in different systems, including human neurons derived from pluripotent cells. They found that 2A specifically cleaved Nup98 and POM121. Using reporter proteins and RNA synthesis and trafficking assays in*

> *cells expressing viral proteases, they showed that 2A induces broad loss of the nuclear pore barrier function, but, surprisingly, the RNA export appears to be minimally affected. Since nucleocytoplasmic trafficking defects are known to be associated with neuropatologies, they propose a hypothesis that 2A-dependent cleavage of nucleoporins in motoneurons underlies the development of EVD68-induced AFM. They further show that a 2A-specific inhibitor increases the survival of human neurons differentiated from stem cells upon EVD68 infection.*
>
> *Strengths:*
>
> *Use of multiple methods to investigate the effect of 2A and 3C expression on nucleoporin cleavage and nucleocytoplasmic trafficking.*

We thank the reviewer for detailed and accurate review of our manuscript and recognition of these strengths.

> *Weaknesses:*
>
> *Overall, the paper follows multiple others that extensively investigated the cleavage of nucleoporins by enterovirus 2As, so the results are of limited novelty. The hypothesis that infection of motoneurons is the cause of EVD68-induced neurological complications so far is supported by only one autopsy report. Other data suggest that infection of other cell types, such as astrocytes, and/or inflammatory cell infiltration in the CNS, are likely to be responsible for the symptoms. In any case, the claim that EVD68 is specifically neurotoxic because of the 2A-dependent cleavage of nucleoporins in neurons is unfounded, as the virus will be just as "toxic" for other infected cell types.*

While we agree that other papers have investigated this pathway in other enteroviruses, we note that our work is the first to do so in Enterovirus D68 and the most comprehensive study, in terms of the number of nucleoporins studied. As we reviewed in paragraph 5 of the introduction section, the activities of enterovirus proteases against specific nucleoporins varies from strain to strain, and is important to understand any strain-specific effects before determining whether this pathway is relevant to toxicity in AFM.

The infection of motor neurons is strongly supported not only by the aforementioned autopsy data [1], but also by mouse model data demonstrating replication of EV-D68 within motor neurons in the anterior horn of the spinal cord.[2] There are also numerous reports of electromyography and nerve conduction studies from human AFM patients demonstrating that the site of pathology is the spinal motor neuron.[3-10]

By contrast, infection of astrocytes has been demonstrated only in primary murine astrocyte cultures in which no neurons were present [11]. Therefore, while the available data suggest that EV-D68 infection of astrocytes is possible, in the *in vivo* context of human and mouse spinal cord, tropism to motor neurons appears to be preferential. The relative toxicity of neuron-autonomous vs non-autonomous processes such as glial dysfunction and inflammatory cell infiltration remain to be elucidated, and are not mutually exclusive.

> *The paper also requires a more convincing presentation of the data.*

We are uncertain what other specific changes the reviewer would like to see based on this comment, but feel that the revisions have improved the presentation of the data.

> ***Reviewer #2 (Public review):***
>
> *Summary:*
>
> *This manuscript investigates the role of EV-D68 proteases 2A and 3C in nuclear pore complex (NPC) dysfunction and their contribution to motor neuron toxicity. The authors*

> *demonstrate that both proteases cleave only a limited number of nucleoporins, with 2A^pro showing the strongest impact by inhibiting nuclear import and export of proteins and disrupting NPC permeability without affecting RNA export. Importantly, treatment with the 2A^pro inhibitor telaprevir reduced neuronal cell death in a dose-dependent manner, achieving neuroprotection at concentrations below those required to inhibit viral replication. The study addresses a relevant mechanism underlying EV-D68-induced neuropathology and explores a potential therapeutic intervention.*
>
> *Strengths:*
>
> *(1) Provides significant mechanistic insight into how EV-D68 proteases alter NPC function and contribute to neuronal toxicity.*
>
> *(2) The use of recombinant 2A and 3C proteins allows clear dissection of the specific contribution of each protease.*
>
> *(3) Demonstrates a therapeutic effect of telaprevir, with neuroprotection independent of viral replication inhibition, adding translational value to the findings.*
>
> *(4) The topic is highly relevant given the association of EV-D68 with acute flaccid myelitis.*

We thank the reviewer for their insightful comments and recognition of these strengths in our study.

> *Weaknesses:*
>
> *(1) Most experiments were performed with recombinant proteases, lacking validation in the context of viral infection, where both proteases act simultaneously.*

In response to this concern, we have added additional experiments in the context of viral infection. We show that POM121 and Nup98 are also cleaved in motor neurons infected with EV-D68 and that their cleavage is inhibited by telaprevir (Fig 4A). We also repeated the EU pulse-chase RNA export assay in EV-D68-infected RD cells and again found no effect on RNA export (Fig 3D-E).

> *(2) The conclusion that RNA export is unaffected requires confirmation during actual infection.*

As above, we have repeated this experiment in EV-D68 RD cells, showing no effect of EV-D68 infection on RNA export.

> *(3) The reduction of neurotoxicity by telaprevir does not fully demonstrate that the protective effect is solely mediated through NPC preservation; additional analyses of eIF4G cleavage, nucleoporin integrity, and stress granules are needed.*

We agree that while the evidence in our manuscript raises the hypothesis that telaprevir-mediated neuroprotection is mediated via NPC preservation, it does not fully demonstrate this to be the case. As discussed above, we have been careful to state only the following conclusions: (1) NPC composition and function is disrupted during EV-D68 infection, (2) $2A^{pro}$ is primarily responsible for functional disruption, and (3) $2A^{pro}$ is neurotoxic.

Future work will determine the extent to which NPC dysfunction contributes to $2A^{pro}$-mediated motor neuron toxicity versus other potential targets of $2A^{pro}$, as suggested by the reviewer. This work is already underway in our lab and it is clear to us the additional experiments required will be extensive, likely 1-2 additional manuscripts. These experiments are therefore beyond the scope of the present study, which represents a key first step in this line of inquiry.

We specifically acknowledged in the Discussion that "A significant limitation of our study, however, is that we cannot exclude potentially toxic effects of $2A^{pro}$ on aspects of host neuronal biology aside from the NPC." We have also made the following adjustments to the text to make it more clear that this remains an open question:

Change the title to more clearly separate the effects of 2Apro on NPC function and motor neuron toxicity as independent events: "Enterovirus D68 2A protease causes nuclear pore complex dysfunction and independently contributes to motor neuron toxicity"

In the abstract, shortened the following sentence: "We therefore sought to determine the impact of EV-D68 proteases on NPC composition and function" to avoid any implicit connection that a mechanistic link has been established between these two concepts. Neurotoxicity is now introduced later in the abstract by saying "Independently, we show…" instead of "We further show…"

Removed language in the last paragraph of the Results section that may have been construed to suggest a mechanistic linkage: "Because similar deficits have been reported to contribute to neurotoxicity in neurodegenerative disease…" and simply stated "We next sought to determine the extent to which 2Apro activity independently contributes to motor neuron injury during EV-D68 infection."

Edited the opening sentence of the discussion, where it was ambiguous whether the word "their" was referring to the enterovirus protease (which was our intent) or to NPC disruption as the cause of motor neuron toxicity. We removed the discussion of toxicity from this paragraph entirely to remove such confusion.

Edited the final paragraph of the discussion to include "We have also demonstrated that $2A^{pro}$ activity contributes to nucleocytoplasmic transport dysfunction and separately to cell death in motor neurons infected with EV-D68". We then go on to discuss the hypothesis that this toxicity might be mediated partially or entirely through NPC dysfunction, and propose that this be a focus of further study.

> *(4) The study would be strengthened by including another 2A inhibitor (e.g., boceprevir) to confirm the specificity of telaprevir's protective effects.*

While we would like to be able to include multiple pharmacologic inhibitors of $2A^{pro}$, unfortunately telaprevir is the only known inhibitor of EV-D68 $2A^{pro}$. The same study that identified telaprevir as an EV-D68 $2A^{pro}$ inhibitor also evaluated boceprevir and determined that its inhibitory activity against $2A^{pro}$ is minimal [12].

> ***Reviewer #3 (Public review):***
>
> *Summary:*
>
> *The author showed expression of the viral proteases 2Apro and 3Cpro of EV-D68, which cleaved specific components of the nuclear pore complex (Nup98 and POM121 by 2Apro), and 2A but not 3C expression altered nuclear import and export. Similar nucleocytoplasmic transport deficits are observed in EV-D68-infected RD cells and iPSC-derived motor neurons (diMNs). 2A inhibitor telaprevir partially rescued the nucleocytoplasmic transport deficits and suppressed neuronal cell death after infection. While it's clear that 2A can cleave NPC proteins and affect nuclear transport, the link to neurotoxicity after EV-D68 infection is less convincing.*
>
> *This study opens up a very intriguing hypothesis: that EV-D68 2Apro could be directly responsible for motor neuron cell death, mediated by POM121 and possibly Nup98 cleavage, that ultimately results in paralysis known as acute flaccid myelitis. This hypothesis notably does run counter to other published data showing that human*

> *neuronal organoids derived from iPSCs can support productive EV-D68 infection for weeks without cell death and that EV-D68-infected mice can have paralysis prevented by depletion of CD8 T cells, still with EV-D68 infection of the spinal cord. However, even if 2Apro is not ultimately responsible for motor neurons dying in human infections, that does not exclude the possibility that cleavage of nups could still disrupt motor neuron function. Notably, most children with AFM have some amount of motor function return after their acute period of paralysis, but most still have some residual paralysis for years to life. It is possible that 2A pro could mediate the acute onset of weakness, while T cells killing neurons could determine the amount of long-term, residual paralysis.*

We thank the reviewer for their thoughtful comments. As discussed above, we agree that the present data demonstrate that $2A^{pro}$ causes NPC dysfunction and is toxic in motor neurons, but has not proven that the mechanism of neurotoxicity is via NPC dysfunction.

We appreciate the commentary on novel hypotheses opened by our work. Our recent thinking on this topic has been similar and we look forward to addressing these ideas further in future studies. Motor neuron dysfunction and motor neuron death may ultimately prove to have separate causes. The infection of motor neurons is likely the initiating event, with multiple downstream consequences which may be neuron-autonomous, or mediated by glial and inflammatory responses, or a mixture thereof.

> *Strengths:*
>
> *The characterization of nuclear pore complex components that appear to be targets of both poliovirus and EV-D68 proteases is quite thorough and expansive, so this data set alone will be useful for reference to the field. And the process by which the authors narrowed their focus to EV-D68 2Apro reducing Nup98 and POM121 as consequential to both import and export of nuclear cargo but not RNA was technically impressive, thorough, and convincing. As will be detailed below, when the authors move from studying over-expressed proteases in transformed cell lines to studying actual virus infection in both transformed cell lines and iPSC-derived neurons, some of the data only indirectly support their conclusions; however, the quality of the experiments performed is still high. So even if the claim that 2Apro causes neurotoxicity is circumstantial, the data certainly are intriguing and certainly justify further study of the effects of EV-D68 2Apro on the NPC and how this impacts pathogenesis. This is a convincing start to an intriguing line of inquiry.*

We appreciate the reviewer's recognition of our comprehensive evaluation of NPC disruption and our approach to arriving at a mechanistic understanding of this process. We agree with the reviewer's viewpoint that the present study represents a beginning, rather than a conclusive end to this line of inquiry. For technical reasons, we were able to achieve more rigorous and mechanistic data in cell lines expressing recombinant proteins than in neurons infected with live virus. In response the reviewers' comments, as described above, we have added additional experiments in this revision in which we further evaluate nucleoporin cleavage and RNA export during live virus infection, and performed these experiments in iPSC-derived neurons whenever it was technically feasible to do so.

> *Weaknesses:*
>
> *This study falls a bit shy of actually showing that 2Apro effects are causing motor neuron toxicity because the evidence of this is fairly indirect. At points, the authors do admit these limitations, but at other times, they claim to have shown the link directly. The following are reasons why these claims are only indirectly supported:*

We agree that we have shown direct toxicity of $2A^{pro}$ in motor neurons, but have not shown that the mechanism is via NPC dysfunction. We felt that we were careful to frame our

conclusions as such. However, we have revised the text to improve the clarity on this point as described above.

> *(1) Cleavage of Nup98 and POM121 after EV-D68 infection in RD cells and diMNs is never demonstrated.*

We have added data showing the cleavage of POM121 and Nup98 in EV-D68 infected diMNs (Figure 4A).

> *(2) Telaprevir was able to rescue nucleocytoplasmic transport in RD cells at low concentrations (Figure 4A). It is not shown if this correlates with its antiviral effect in RD cells, or could this correlate with inhibition of 2A cleavage of Nup98 or POM121, which is never measured.*

In the aforementioned new experiment in Figure 4A, we have also included a dose-response curve for telaprevir showing its inhibition of POM121 and Nup98 cleavage.

> *(3) Building off of the prior point, the authors' claim that the neuroprotective effect of telaprevir is independent of its antiviral effect is not well-founded. Figure 4E (neuroprotection) was done with MOI 5, and Figure 4G (virus growth) was MOI 0.5. Telaprevir neuroprotection is not shown at MOI 0.5, nor is the neuroprotective effect correlated with inhibition of 2A cleavage of Nup98 or POM121.*

The selection of MOIs for these two experiments was limited by technical considerations. If the viral growth curve were to be performed at MOI 5, it would be confounded by cell death. Further, a low MOI is required in order to allow multiple rounds of infection, and is therefore more sensitive for assaying the effect of telaprevir on viral replication. On the other hand, at MOI 0.5 diMN death is very gradual, and the neuroprotection assay we would have lacked the statistical power to determine whether a rescue of this small magnitude of toxicity is significant. The EC_{50} of telaprevir is not expected to vary at different MOIs.

We have also now correlated the inhibition of $2A^{pro}$ cleavage of Nup98 and POM121 with the neuroprotective effect at comparable concentrations of telaprevir, as described above.

> *(4) The use of mixed virus isolates only in the diMNs is problematic because different EV-D68 isolates are known to have drastically different effects on pathogenesis in mice. Since all initial data were generated with the MO isolate, adding the additional MD isolate to the diMN experiments actually adds uncertainty to the conclusions. It is not clear if the authors infected different cultures with the different isolates and combined the data or infected all cultures with a mixture of the two isolates. If the former, then the data should be reported separately to see the effect of each individual strain, which would be interesting to EV-D68 virologists. If the latter, then there is no way to know from these data whether one of the two isolates had increased fitness over the other and exerted a dominant effect. If the MD isolate overtook the MO isolate, from which all other data in this manuscript are derived, then we have much less of an idea how much the data from the first three figures supports the final figure.*

We apologize for the lack of clarity in describing this experiment. The MO/2014 and MD/2018 isolates were not mixed. These were performed in separate experiments, each with four biologically independent replicates. The original figure showed the mean and SEM for these 8 replicates together. To improve clarity, we separated each viral strain into its own panel of the figure. We have also increased the rigor of the statistical analysis in this experiment by using Cox proportional hazard regression instead of ANOVA.

> ***Recommendations for the authors:***
>
> ***Reviewing Editor Comments:***

> *Please consider both public reviews above and recommendations for the authors below. The general consensus among reviewers is that more evidence is needed to support the claim that 2A causes motor neuron toxicity during infection.*
>
> ***Reviewer #1 (Recommendations for the authors):***
>
> *Most of the conclusions are made upon analysis of images, yet the images themselves are seldom shown. It is difficult to evaluate the validity of conclusions without seeing the material that was analyzed.*
>
> *(1) Figure 1. Representative Western blots should be shown.*

We considered including representative western blots in this already large figure, however the figure size and complexity became un-manageable because the figure summarizes the quantification of 246 Western blots. In the original submission, we uploaded a supporting data file that included complete un-cropped Western blots for all experiments, including ladders, loading controls, and clear labeling of the samples. We believe these data allow the reader to assess the quality and reliability of our Western blot experiments while maintaining the approachability of the figures and data presentation. We have also included these supporting data again in the revised manuscript.

> *(2) Figure 3. Representative images should be shown. This is especially important for the ethynyl-uridine labeling experiment. It would be highly surprising that RNA transcription and processing would proceed normally in 2A-expressing cells on the background of a major redistribution of nuclear proteins. One possible explanation for that would be that cells that can be analyzed express a relatively small amount of 2A, which is known to be toxic, and thus may not fully represent the cellular changes upon infection. The results from bona fide infected cells would be much more convincing.*

Representative images have been added for the ethynyl-uridine pulse-chase experiment, and this experiment has been repeated in RD cells infected with EV-D68. Transfection of proteases or infection of the cells utilized the same protocols and timeframes upon which nucleoporin cleavage and disruption of protein transport were found to be present. The timepoint for all of these experiments was selected to precede the onset of toxicity, and the representative images demonstrate normal cellular morphology. We also selected for analysis only GFP+ cells with normal morphology, ensuring that only viable $2A^{pro}$-GFP-expressing cells were included in the analysis. The new experiments again showed no effect on RNA export. We were equally surprised as the reviewers by this outcome. However, as we note in the text, disruption of RNA export has not been uniformly present across all enteroviruses previously studied.

> *(3) Figure 4 A-D. Similarly, representative images should be shown.*

We have added representative images for these experiments, which are now Fig 4B-E.

> *(4) Figure 4G. The demonstration that the "neuroprotective" effect of 2A inhibitor is not related to the inhibition of viral replication requires a control showing that a similar inhibition of viral replication by an inhibitor with another target would not similarly diminish cell toxicity.*

Neuronal survival experiments showed inhibition of toxicity with concentrations of telaprevir as low as 0.3 uM, a concentration at which there was no significant effect on viral replication. Telaprevir had only a marginal inhibitory effect on viral replication at 10uM (achieving statistical significance in only one of two strains), and no consistent effect on replication at lower concentrations. Therefore, the suggested control experiment would not

be possible, because the neuroprotective concentration of telaprevir does not inhibit viral replication

> ***Reviewer #2 (Recommendations for the authors):***
>
> *Major concerns:*
>
> *(1) Most of the experiments were performed with recombinant 2A and 3C proteins. While these experiments are highly informative for dissecting the role of each protease in NPC dysfunction, it would be important to also perform experiments in the context of infection. How are import and export processes affected when both proteases are present during infection? How is passive transport modified under these conditions?*

Thank you for this important comment. Please see the above discussion of additional experiments that we added utilizing live virus infection to complement the experiments that used recombinant proteins.

> *(2) The results regarding RNA export in the presence of recombinant 2A and 3C proteases suggest that RNA export is not altered. It would be important to confirm this finding during infection.*

We agree that this is an important experiment, and have done so as described above.

> *(3) While the background information suggests that NPC dysfunction contributes to neurotoxicity, the observed reduction of neurotoxicity by telaprevir does not demonstrate that this effect is solely due to the action of 2A on the NPC. It would be important to evaluate the integrity of eIF4G, nucleoporins, and stress granules during treatment.*

We agree that additional experiments would be required to determine the extent to which the toxicity of $2A^{pro}$ is mediated through its effects on the NPC versus other potential targets. Please see above discussion for more details.

> *(4) Including another 2A inhibitor (e.g., boceprevir) would strengthen the conclusions by confirming the results obtained with telaprevir.*

Please see above discussion of boceprevir

> ***Reviewer #3 (Recommendations for the authors):***
>
> *(1) Preferred ICTV nomenclature abbreviates rhinovirus as RV instead of HRV, so the authors should change their abbreviations appropriately. See Simmonds et al.*
>
> *Archives of Virology (2020) 165:793-797 https://doi.org/10.1007/s00705-019-04520-6*

We have updated these abbreviations accordingly.

> *(2) There is no mention of Figures 1C and 1D in the text.*

These have been added in the appropriate locations.

> *(3) In the section "2A protease alters nucleocytoplasmic trafficking of protein substrates" it would be very helpful to just directly state what each construct is meant to demonstrate. Along the lines of "NLS-tdTomato should be located in the nucleus, so seeing more signal in the cytoplasm would indicate a defect in nuclear import." And something equivalent for the other two constructs.*

Thank you for the suggestion. We have added descriptions of the use and interpretation for each construct.

> *(4) The following sentence would be more accurate with the addition of "partially" because the effect is not returned to normal levels: "The mislocalization of NLS-tdTomato was partially rescued by 3μM telaprevir."*

We have edited this as recommended.

> *(5) SNAP29 is probably a typo and meant to be CREB in the legend of Figure 1B.*

Thank you for catching this. We have corrected this to CREB.

> *(6) "Panel A" should likely be "Panel E" in the Figure 4F legend.*

We have corrected this to refer to the appropriate panel, which has also been re-lettered due to the addition of new panels to this figure.

> *(7) The authors should at least show representative Western blot data used to determine the data for Figure 1 in a supplemental figure.*

As discussed above, these Western blots were included as supplemental data in the original submission, and have also been included in the revised version.

> *(8) As suggested in the public comments, if the diMNs were infected separately with the MO and MD strains of EV-D68, those data should be separated from each other and reported individually. In any case, whatever was done (combined virus inoculum or separate inocula) needs to be clarified.*

These data are now reported separately. Please see above discussion for details.

References:

(1) Vogt MR, Wright PF, Hickey WF, De Buysscher T, Boyd KL, Crowe JE, Jr. Enterovirus D68 in the Anterior Horn Cells of a Child with Acute Flaccid Myelitis. N Engl J Med. May 26 2022;386(21):2059-2060. doi:10.1056/NEJMc2118155

(2) Hixon AM, Yu G, Leser JS, et al. A mouse model of paralytic myelitis caused by enterovirus D68. PLoS Pathog. Feb 2017;13(2):e1006199. doi:10.1371/journal.ppat.1006199

(3) Andersen EW, Kornberg AJ, Freeman JL, Leventer RJ, Ryan MM. Acute flaccid myelitis in childhood: a retrospective cohort study. Eur J Neurol. Aug 2017;24(8):1077-1083. doi:10.1111/ene.13345

(4) Elrick MJ, Gordon-Lipkin E, Crawford TO, et al. Clinical Subpopulations in a Sample of North American Children Diagnosed With Acute Flaccid Myelitis, 2012-2016. JAMA Pediatr. Feb 1 2018;173(2):134-139. doi:10.1001/jamapediatrics.2018.4890

(5) Hovden IA, Pfeiffer HC. Electrodiagnostic findings in acute flaccid myelitis related to enterovirus D68. Muscle Nerve. Nov 2015;52(5):909-10. doi:10.1002/mus.24738

(6) Knoester M, Helfferich J, Poelman R, et al. Twenty-Nine Cases of Enterovirus-D68 Associated Acute Flaccid Myelitis in Europe 2016; A Case Series and Epidemiologic Overview. Pediatr Infect Dis J. Jan 2018;38(1):16-21. doi:10.1097/INF.0000000000002188

(7) Martin JA, Messacar K, Yang ML, et al. Outcomes of Colorado children with acute flaccid myelitis at 1 year. Neurology. Jul 11 2017;89(2):129-137. doi:10.1212/WNL.0000000000004081

(8) Saltzman EB, Rancy SK, Sneag DB, Feinberg Md JH, Lange DJ, Wolfe SW. Nerve Transfers for Enterovirus D68-Associated Acute Flaccid Myelitis: A Case Series. Pediatr Neurol. Nov 2018;88:25-30. doi:10.1016/j.pediatrneurol.2018.07.018

(9) Van Haren K, Ayscue P, Waubant E, et al. Acute Flaccid Myelitis of Unknown Etiology in California, 2012-2015. JAMA. Dec 22-29 2015;314(24):2663-71. doi:10.1001/jama.2015.17275

(10) Natera-de Benito D, Berciano J, Garcia A, E MdL, Ortez C, Nascimento A. Acute Flaccid Myelitis With Early, Severe Compound Muscle Action Potential Amplitude Reduction: A 3-Year Follow-up of a Child Patient. J Clin Neuromuscul Dis. Dec 2018;20(2):100-101. doi:10.1097/CND.0000000000000217

(11) Rosenfeld AB, Warren AL, Racaniello VR. Neurotropism of Enterovirus D68 Isolates Is Independent of Sialic Acid and Is Not a Recently Acquired Phenotype. Mbio. 2019;doi:10.1128/mBio

(12) Musharrafieh R, Ma C, Zhang J, et al. Validating Enterovirus D68-2A(pro) as an Antiviral Drug Target and the Discovery of Telaprevir as a Potent D68-2A(pro) Inhibitor. J Virol. Jan 23 2019;doi:10.1128/JVI.02221-18

https://doi.org/10.7554/eLife.108672.2.sa0